

Review

Electrochemical Sweat Sensors

Emanuel Bilbao ¹, Octavio Garate ¹, Theo Rodríguez Campos ^{1,2}, Mariano Roberti ³, Mijal Mass ³, Alex Lozano ^{1,3}, Gloria Longinotti ¹, Leandro Monsalve ^{1,4} and Gabriel Ybarra ^{1,*}

- ¹ Functional Nanomaterials Group, INTI-Micro and Nanotechnologies, National Institute of Industrial Technology, Av. Gral. Paz 5445, San Martín B1650WAB, Argentina; ebilbao@inti.gov.ar (E.B.); ogarate@inti.gov.ar (O.G.); trodriguez@inti.gov.ar (T.R.C.); alozano@inti.gov.ar (A.L.); mlonginotti@inti.gov.ar (G.L.); monsalve@inti.gov.ar (L.M.)
- ² Institute for Industrial Quality (INCALIN) (INTI—UNSAM), Av. Gral. Paz 5445, San Martín B1650WAB, Argentina
- ³ Printed Electronics & Rapid Prototyping Group, INTI-Micro and Nanotechnologies, National Institute of Industrial Technology, Av. Gral. Paz 5445, San Martín B1650WAB, Argentina; froberti@inti.gov.ar (M.R.); mmass@inti.gov.ar (M.M.)
- ⁴ CONICET—INTI—UNSAM, Av. Gral. Paz 5445, San Martín B1650WAB, Argentina
- * Correspondence: gybarra@inti.gov.ar

Abstract: Sweat analysis by means of minimally invasive wearable sensors is considered a potentially disruptive method for assessing clinical parameters, with exciting applications in early medical diagnostics and high-performance sports. Electrochemical sensors and biosensors are especially attractive because of the possibility of the electronic integration of wearable devices. In this article, we review several aspects regarding the potentialities and present limitations of electrochemical sweat (bio)sensors, including: the main target analytes and their relationships with clinical conditions; most usual electrochemical techniques of transduction used according to the nature of the target analytes; issues connected to the collection of representative sweat samples; aspects regarding the associated, miniaturized electronic instrumentation used for signal processing and communication; and signal processing by machine learning.

Keywords: diagnostics; electrochemical biosensors; potentiometric sensors; sweat analysis



Citation: Bilbao, E.; Garate, O.; Rodríguez Campos, T.; Roberti, M.; Mass, M.; Lozano, A.; Longinotti, G.; Monsalve, L.; Ybarra, G. Electrochemical Sweat Sensors. *Chemosensors* **2023**, *11*, 244. <https://doi.org/10.3390/chemosensors11040244>

Academic Editor: Gabriela Broncová

Received: 20 January 2023

Revised: 1 April 2023

Accepted: 3 April 2023

Published: 14 April 2023



Copyright: © 2023 by the authors. Licensee MDPI, Basel, Switzerland. This article is an open access article distributed under the terms and conditions of the Creative Commons Attribution (CC BY) license (<https://creativecommons.org/licenses/by/4.0/>).

1. Introduction

1.1. Electrochemical Biosensing of Sweat Composition as a Diagnostic Tool

Eccrine sweat is an aqueous biofluid excreted by millions of glands distributed all over the human body. These glands have an important thermoregulator role and excretory functions aiming to eliminate excess wastes and toxicants [1]. Eccrine sweat is mostly composed of electrolytes and metabolites, but it also contains vitamins, hormones, peptides, and macromolecules in lower concentrations [2]. The composition of sweat can be related to the physiological human body status and clinical conditions (Table 1). For instance, chloride sweat concentration measurement is the gold standard for cystic fibrosis detection [2], glucose level monitoring is crucial for healthy control of diabetic patients, and sweat lactate level measurements could be a good candidate for sport physiology assessment [3].

The compounds of interest present in sweat can be determined using electrochemical sensors and biosensors. The detection approach used in each case is greatly determined by the nature of the analyte, which we can roughly classify into three kinds: electrolytes, small organic molecules, and macromolecules and intermediate-size (bio)molecules (proteins, steroid hormones, and so on). For instance, ion-sensitive electrodes are the technique of choice for the selective determination of ions in concentrations higher than 1 mM. Ions in low concentration (heavy metals such as Zn, Cd, Pb, Cu and Hg, present at trace levels) have also been detected, albeit by employing more sensitive voltammetric techniques, such as square wave anodic stripping voltammetry [4]. Similarly, the standard means

of electrochemical determination of the concentrations of small organic molecules (e.g., glucose, lactate, ethanol, etc.) is amperometric enzymatic biosensing. Redox enzymes are used to specifically detect the substrate (analyte), and its catalytic activity (reaction rate) is converted into an electronic current proportional to the analyte concentration. Finally, affinity biosensors are the preferred choice in cases of intermediate-size (bio)molecules and macromolecules. The occurrence of antigen-antibody events is electrochemically detected (usually by means of a voltammetric technique or by electrochemical impedance spectroscopy, EIS) on the surface of a sensing electrode, where the biorecognition element (either the antigen or the antibody) has been immobilized.

Table 1. Key analytes in sweat and the related detection methods. Adapted with permission from Refs. [5], Copyright 2021, and [6], Copyright 2023.

Target Analyte	Concentration in Sweat	Disease Correlation	Sensing Modality	Ref.
Ions	Na ⁺	10–100 mM	Ion-selective potentiometry	[7,8]
	Cl [−]	10–100 mM		[7,9]
	K ⁺	1–18.5 mM		[7]
	Ca ²⁺	0.41–12.4 mM		[9]
	pH	3–8		[10]
	NH ₄ ⁺	0.1–1 mM		[10]
Metabolites	Glucose	10–200 μM	Amperometric enzymatic biosensors	[7]
	Lactate	5–20 mM		[11]
	Ethanol	2–30 mM		[12]
	Uric acid	2–10 mM		[13]
	Ascorbic acid	10–50 μM		[13]
Hormones	Cortisol	22–390 nM	Voltammetry, electrochemical impedance spectroscopy	[14]
Macromolecules	Peptides Proteins (antibodies, antigens, enzymes)	-	Square wave voltammetry, electrochemical impedance spectroscopy	

Especially attractive is the possibility of minimally invasive analysis provided by wearable electrochemical sweat sensors. Wearable devices (or simply wearables) are autonomous, non-invasive, and on-body devices aiming to collect and analyse data. They are usually incorporated into smartwatches, glasses, earbuds, skin stickers or tattoos, patches, and jewellery. Health wearables perform specific healthcare functions, such as the measurement of physiological parameters. These wearables incorporate mechanical, chemical, and biochemical sensors to monitor physical parameters and key analytes or biomarkers in biofluids. In all instances, smart sensors, artificial intelligence (AI), big data, and internet of things (IoT) technologies may be implied to acquire, process, and wirelessly transmit health condition information to the user or healthcare provider, using this powerful tool for disease management, diagnosis, prediction, and follow-up [15].

1.2. Key Health-Related Examples of Sweat Biochemical Analysis

Cystic fibrosis (CF) is a genetic disorder characterized by the production of thick and sticky mucus due to elevated concentrations of chloride in extracellular liquid that affects the lungs, pancreas, and other organs. Sweat testing is considered the gold standard for CF diagnosis. Sweat is collected, and its level of chloride concentration is measured.

Levels higher than 60 mM are consistent with the diagnosis of CF. According to Cystic Fibrosis Foundation guidelines, sweat must be quantitatively analysed for chloride by electrochemical methods or by automated analysers using ion-selective electrodes [16].

Glucose monitoring systems can be classified as invasive, minimally invasive, and non-invasive. The standard finger-prick test to determine the level of glucose in blood and the interstitial fluid glucose sensor, which are commercially available and highly diffused, can be considered invasive and minimally invasive, respectively. Even though blood testing is considered the gold standard, there is a trend toward migrating to less invasive and painless techniques for analysing alternative biofluids, such as saliva, tears, and sweat. Sweat-based sensors are considered the least invasive method to assess glucose levels. Moyer et al. [17] reported that there is a statically significant correlation between glucose concentrations in blood and in sweat, with glucose present in sweat representing about 1–2% of the glucose in blood. However, Moyer and most of the other authors affirmed that the greatest technological challenge of this alternative technique is to acquire a representative and interferent-free sweat sample to obtain accurate measurements.

Rapid detection and precise monitoring of therapeutic and non-legal drugs are essential for the healthcare system due to the current high level of substance abuse. Some researchers work on the development of innovative systems for drug monitoring based on sweat sensors. Xue et al. [18] developed a microfluidic system based on a competitive ELISA technique to detect drug-related metabolites in sweat. They reported a rapid system to quantify, in around 16 min, methadone, methamphetamine, amphetamine, and THC using approx. 4 μL of sweat. Moreover, Tai et al. [19] implemented a methylxanthine drug-monitoring wearable platform equipped with an electrochemical differential pulse voltammetry sensing module with sensitivity of 110 $\text{nA } \mu\text{M}^{-1}$. In addition, Teymourian et al. [20] included in their review the detection in sweat of heroin and its metabolites, codeine, fentanyl, methadone, cocaine and its metabolites, ethanol, and amphetamine-type stimulants, in the order of nanograms to a few micrograms.

Sport technologies were introduced to help users to reach their desired fitness level or maximum potential. Sports and wellness sensors, which are mostly wearable, gather information about the physiological wearers' status, their performance, and the environmental conditions [21]. Sweat sensors are relevant in sports applications because the monitoring of sweat composition variations along training routines could provide enough information to assess athletes' status and personalize their training. Parrilla et al. [22] developed a potentiometric ion patch based on multiple-wall carbon nanotubes (MWCNTs) electrodes to monitor pH, Cl^- , K^+ , and Na^+ in sweat. Researchers have paid special attention to lactate because, first, its sweat concentration is higher than its blood concentration [3] and, second, because there is a possible correlation between its concentration and exercise intensity [23]. For instance, Zhang et al. [24] developed a wearable enzymatic lactate biosensor mounted on eyeglasses. This device presented a linear response up to 25 mM in a phosphate-buffered solution with a pH of 7.

2. Sampling Techniques

2.1. Traditional Methods of Sampling Sweat

In traditional analysis under laboratory conditions, sampling or collection is also a crucial step in sweat analysis due to its great impact on the accuracy of the determination of electrolyte and metabolite concentrations [25]. In all instances, the procedures require trained operators and must satisfy biosecurity requirements to avoid producing injuries to the user and contaminating the sample.

Traditional sampling methods include systemic and local methods. The systemic method is the whole-body wash-down, and it is considered the gold standard for whole body loss of Na^+ and other electrolytes [25]. As its name suggests, it consists of washing with deionized water the whole body, the user's clothes, and the equipment before and after an exercise routine in a closed system under controlled conditions. The sample

obtained is a interferent-free biofluid, and the normal evaporative process is maintained undisturbed [25].

Local methods include patches, polymer bags and films, scraping/ripping/gathering, and macroducts. Patches are a low-cost, flexible, in-body, and disposable alternative to collect local sweat in a hydrophilic porous structure [25]. Polymer bags and films involve a simple and disposable method to collect sweat. They usually consist of an adhesive rubber that covers the skin and a polymeric bag to accumulate the biofluid. In the scraping/dripping/gathering method, sweat is collected in capillary tubes, test tubes, or beakers. Even though it is a simple and inexpensive method, there are many sources of potential error, especially due to evaporation and contamination. Macroducts are commercial disposable products mostly used in CF diagnosis that consist of a spiral plastic tube to collect sweat. The collecting procedure takes at least 30 min.

2.2. Sampling Methods for Wearable Systems: Sweat Generation and Collection

Wearable sensors for continuous or intermittent monitoring of biomolecules from body fluids are highly desired as integrated platforms in the human body [26]. Some of the desired properties of the new wearable sensors are stretchability, ultra-thinness, biocompatibility, biodegradability, and self-healing [27]. For example, since a sweat collecting system is in direct contact with the skin, it should be fabricated from a smooth, non-irritating, and anti-allergic material so that it does not generate inflammation on the skin after wearing the sensors.

Wearable devices have evolved gradually with a mix of multiplexed biosensing, microfluidic sampling, and transport systems integrated with flexible materials and body attachments for improved wearability and simplicity [28]. These wearables hold promise and are capable of greater understanding of the correlations between analyte concentrations within the blood or non-invasive biofluids and feedback to the patient, which is significantly important in timely diagnosis, treatment, and control of medical conditions [28].

Sweat sensors offers an innovative and non-invasive alternative for physiological monitoring. With adequately processed data by AI and big data techniques, they could be a powerful tool to guide clinical decision-making. However, even though the field of electrochemical sensors and biosensors is mature, measuring sweat samples presents several challenges, especially regarding wearable sweat sensors. For instance, the lifetime of wearable electrochemical biosensors is significantly dependent on the long-term stability of functional materials modified on the flexible substrate, the effect of pH changes in sweat on the sensing device, and signal fluctuations caused by the bending of sensors. For all applications, researchers and developers agree that the main drawback of sweat sensors is obtaining a sufficient sample of sweat in a short period time that represents the physiological status of the human body without interferents and contaminants [3]. Therefore, sampling is a key point for the development of sweat sensors.

The extraction of a representative sample involves two processes: sweat generation, followed by efficient collection.

With respect to sweat generation, sweat glands can be stimulated by steam or dry heat exposition (thermal stimulation) and exercise. Thus, in the case of sweat analysis of athletes, sweating is spontaneously produced by physical exercise. However, for health-related sweat analysis, patients are usually at rest, and sweating must be artificially and locally generated. One of the most commonly used pharmacological techniques to stimulate sweating is iontophoresis [1]. Iontophoresis is an established process used to induce ion/molecular flow by applying a mild electric current across the skin, and it is widely used in clinics for diagnostic and therapeutic purposes [2]. Iontophoretic transdermal drug delivery is used to distribute agonist drugs (e.g., pilocarpine, carbachol, or lidocaine) from an electrode across the skin (Figure 1). However, in some cases, the iontophoretic drug may interfere with the electrochemical determination. Thus, a protective layer of agarose on top of the electrode has been implemented to avoid drug-related interference [29].

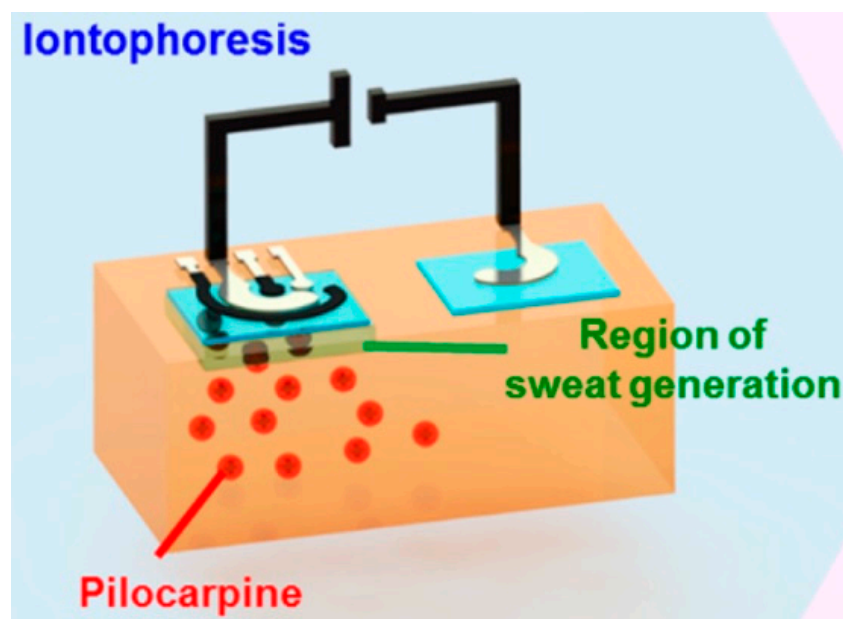


Figure 1. Schematic diagram of an iontophoretic-sensing tattoo device, containing the iontophoretic electrodes (IEs; anode and cathode) and three sensing electrodes (working, reference, and counter electrodes: WE, RE, and CE, respectively). Reprinted with permission from [12]. Copyright (2016), American Chemical Society.

The acquisition of representative samples requires sweat to be efficiently collected and transported to the sensing electrode. Several approaches and materials have been employed to achieve this end, involving the use of functional absorbent materials, superhydrophobic/superhydrophilic surfaces, sweat guidance, and epidermal microfluidic systems.

First, absorbent materials, such as nonwoven fabrics, papers, and hydrogels, accumulate sweat in their pores and efficiently guide it to the sensor surface. Furthermore, these materials can be functionalized with selective components. For instance, Li et al. [30] developed a sensing platform for real-time sweat analysis combining paper, hydrophobic wax, conducting electrodes, and active materials (MXene/methylene blue). As result, a sweat-based glucose and lactate sensor with sensitivity $2.4 \text{ nA } \mu\text{M}^{-1}$ was developed.

Second, surface wettability can be modified to collect, accumulate, and directionally transport sweat samples from superhydrophobic to superhydrophilic zones. For instance, He et al. [31] developed a band aid that combines superhydrophobic and superhydrophilic microarrays with colorimetric biosensors for sweat assessment. In addition, Dai et al. [32] modified a Janus fabric surface, obtaining an array of hydrophilic pores to unidirectionally pump accumulated sweat.

Third, researchers have developed more sophisticated and innovative methods to drive biofluid to the sensor system through microchannels in polymeric substrates, for example, polydimethylsiloxane (PDMS). Sweat flows through the channels thanks to capillary action and the pressure of the hydraulic pumping action of sweat glands [25].

Finally, microfluidic systems are a trend in wearable development. Researchers have combined sensors, microfluidics, and electronics into on-body devices. However, Hoovels et al. [25] reported that it is not trivial to find wearable devices that properly function on a microfluidic basis to analyse sweat. Cao et al. proposed a three-dimensional paper-based microfluidic electrochemical integrated device for real-time monitoring of sweat metabolites and electrolytes (Figure 2). The collector had five stacked layers: a sweat collector, a vertical channel, a transverse channel, an electrode layer, and a sweat evaporator. Beyond these components, the capillary effect of paper helps the sweat to flow into the paper-based devices, contributing to sweat collection.

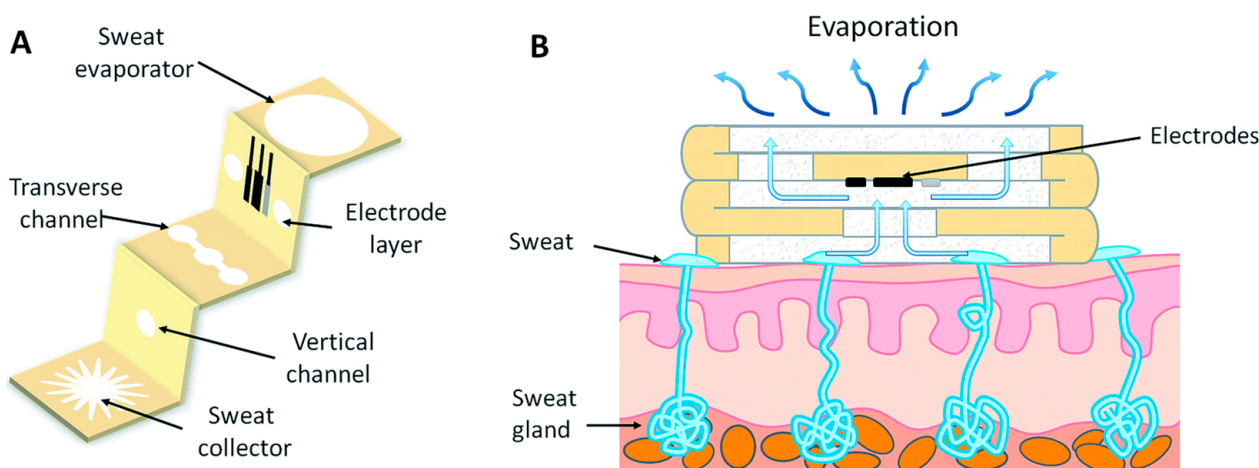


Figure 2. Schematic diagram of the three-dimensional paper-based microfluidic electrochemical integrated device. (A) The layered structure of the device. 3D-PMED includes the sweat collector, vertical channel, transverse channel, electrode layer, and sweat evaporator. The yellow areas or the white areas on the device were hydrophobic areas formed by wax screen-printing or hydrophilic areas of filter paper, respectively. A three-electrode electrochemical sensor created by screen-printing was affixed on the electrode layer of the device using double-sided adhesive tape. (B) The schematic diagram of the 3D-PMED applied on the skin of a human. A 3D-flow channel was formed by folding the device with the tiered structure to help the sweat to flow from the skin into the device and thus refresh the sweat under the electrodes. Reproduced with permission from Ref. [33], Copyright 2019, RSC.

Sweat collection remains an important topic in wearable sensors, as the fluid flow under the patch is important for real-time, continuous analysis of sweat and long-term comfort of the skin. Additionally, sweat accumulation under sensors will cause skin discomfort [18].

3. Sensing Electrolytes in Sweat with Potentiometric Ion-Selective Electrodes

As previously detailed, electrolytes are among the most targeted biomarkers within sweat analytics due to their roles in hydration, osmotic balance, and muscle stimulation. Within the proposed sensing techniques, amperometry, potentiometry, and conductometry stand out as both suitable and relevant candidates. However, potentiometry is the most commonly used technique for the determination of electrolytes with electrochemical sweat sensors.

Potentiometry is a technique that allows for electrolyte quantification according to the Nernst equation, even at relatively low concentrations of sweat, based on the use of a dual probe sensor composed of an ion-selective electrode (ISE) and a reference electrode (RE). Recent advances in the field of flexible and printable electronics, nanomaterial synthesis, and chemical functionalization have laid a solid foundation to overcome the limitations of proof-of-concept approaches and develop sensors as skin-mounted systems through drop casting (DC), screen printing (SP), or ink-jet printing (IJP) [34,35].

Drop casting is a simple film-forming technique proposed by many researchers to develop a diverse array of electrochemical sensors without the need for specific equipment. Regarding REs, this accessible methodology is used to chemically modify the surfaces of commercial screen printed or solid-state electrodes through a simple process of casting a solution containing the desired material over the desired electrode surface, resulting in a layer after solvent evaporation [36].

On the other hand, inkjet printing and screen printing have been reported as the most promising approaches for simple, fast, and inexpensive production of sensing platforms. Their cutting edge technologies can be attributed to the miniaturization of electrochemical sensors, reducing the sample volume required to as little as a few microliters, allowing for the size reduction of the diagnostic platform into which they are integrated. Furthermore,

the as-obtained screen-printed (SPEs) or inkjet-printed electrodes (IJPES) can be further and easily functionalized through physicochemical procedures to confer qualities such as specificity, selectivity, and stability. Alongside the previously mentioned advantages, SP and IJP mass production capabilities encompass the totality of their potentialities, justifying SP and IJP as suitable candidates complying with the ongoing demands for rapid and accurate in-situ analyses through portable devices. Adapting conventional ISE and RE to these techniques represents a hindrance, for example, the constant attempts by the scientific community to develop a robust and low-cost alternative to the conventional glass silver/silver chloride (Ag/AgCl) gel RE [37].

Considering the functional importance of both ISE and RE, the following section addresses structural, performative, and suitability characteristics, allowing, at the end, for the presentation of a general conclusion regarding the state of ISE and RE development and the pending challenges that have yet to be overcome.

3.1. Reference Electrode

The Ag/AgCl electrode is almost universally used as a reference electrode in electrochemical sweat sensors. There are several reasons for this choice: biocompatibility of the materials, compatibility with the sweat's pH, and commercially available inks for SP and IJP. Therefore, we consider exclusively the Ag/AgCl RE in this section.

As illustrated in Figure 3a, the conventional RE is structurally composed of a glass vessel containing a silver wire coated with silver chloride, immersed in a KCl solution with a constant concentration. Potassium chloride is generally used as the electrolyte because K^+ and Cl^- present similar high mobilities, which improve the overall transient response of the RE.

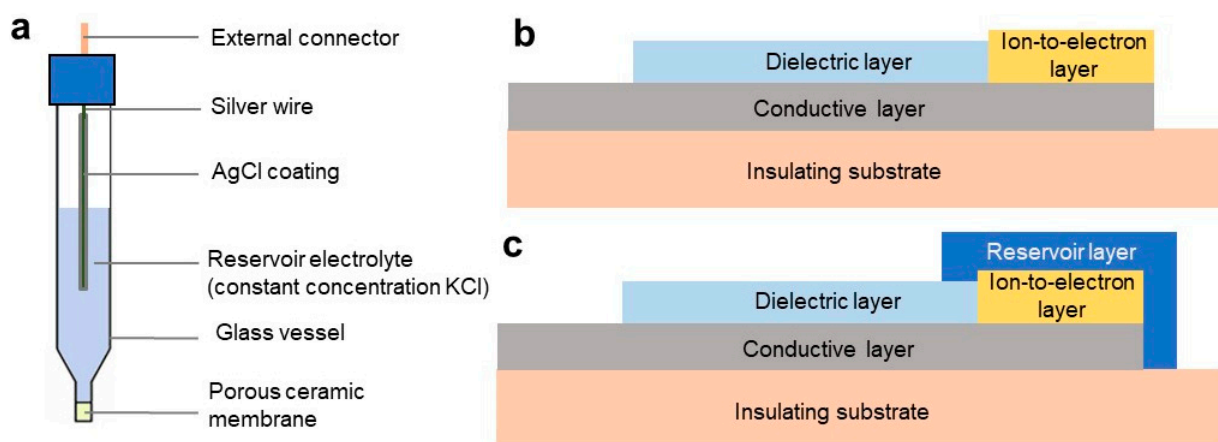
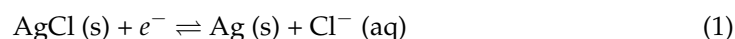


Figure 3. (a) Illustration of the components present in a traditional reference electrode. (b,c) Stratified view presenting structural differences between a printed pseudo-reference electrode (b) and a printed reference electrode (c).

From an operational standpoint, classical Ag/AgCl RE features a reversible electron transfer reaction involving a slightly soluble salt (AgCl) and a metallic electrode (Ag):



As a product of this reaction, if the chloride concentration is kept constant, an unequivocal and stable electrode potential is defined following the Nernst equation:

$$E = E^0 - 2.3 RT/zF \log [Cl^-] \quad (2)$$

where E^0 is the electrode standard half-cell potential (V), R is the molar gas constant ($J K^{-1} mol^{-1}$), T is the absolute temperature (K), z is the number of involved electrons transferred in the half-reaction, F is the Faraday constant ($C mol^{-1}$), and $[Cl^-]$ is the

concentration of chloride ions (M). Under this thermodynamic correlation, a conventional Ag/AgCl electrode displays, at a temperature of 25 °C, a $[\text{Cl}^-]$ dependent Nernstian response of -59.16 mV/pCl . In addition, conditions of KCl oversaturation (between 3.5 M and 4 M) ensure a stable half-cell potential in a broad spectrum of solutions, a desirable quality for any RE.

Recent publications have indicated that the RE is an essential component in any potentiometric device since the response of an ISE is meaningless without a reference against which to compare it [38–45]. Additionally, replicating both the structural and the functional characteristics of a conventional RE in portable or wearable ISEs is not a trifling matter since DC, SP, and IJP are the methodologies selected in recent times to develop REs that meet the technical requirements of this type of device.

3.1.1. Reference Electrodes: Structural Overview

As stated previously, the REs constructed using DC are based on a layered modification of commercial SC or solid-state electrodes as base templates (further details can be found in Section 3.1.3). As a result, the following structural overview addresses, for simplicity's sake, the three approaches (DC, SP, and IJP) considering the RE as a bottom-up layered structure (Figure 3b,c).

The first reported Ag/AgCl REs presented up to three distinct functional layers [46,47]. The first layer is conductive and is responsible for allowing efficient electron transfer while closing the electrical circuit. The second layer, referred as to the ion-to-electron layer, is the one that contains Ag/AgCl and establishes a reference potential, as explained above (Equations (1) and (2)). In addition to this basic two-layered structure, an additional layer (the dielectric layer) is required for printed reference electrodes (PREs) to control the functional area of each layer exposed to the measurement solution and to protect the electrical connections pads.

Unfortunately, there is no component in its structure to offset the dilution-induced decrease in $[\text{Cl}^-]$ with time, which results in subsequent potential fluctuations, as indicated by the Nernst equation. These characteristics are those of a pseudo-reference electrode, limiting its field applications since environmental and human samples contain either proteins or anions that affect the stability of their electrochemical potential considerably.

Considering all the limitations of the proposed approaches using pseudo-reference electrodes, the next step in RE development was aimed at printing or casting any necessary additional layers to improve reproducibility, repeatability, lifetime, and chloride ion concentration susceptibility, with its performance resembling that of a traditional electrode glass Ag/AgCl gel RE. Concerning this development, Andrade et al. [48] provided an alternative for RE development that would solve the limitations of pseudo-reference electrodes. In their work, the authors presented a glassy carbon (GC) drop casted RE, containing a layer of Ag/AgCl alongside a membrane cocktail of polyvinyl butyral (PVB) and NaCl. The RE showed a stable potential over a wide range of concentrations for several chemical species, no significant drift, and a considerable lifetime of four months.

The reason why this electrode presented similar performance compared with a conventional double-junction reference electrode can be interpreted from the standalone functionality of its components. First, the Ag/AgCl layer governs, in the absence of any secondary redox couples, the ion-to-electron transduction process. Second, an excess of chloride ions near the RE surface provides constant potential over time. However, this statement is only correct if the concentration of chloride reaches a steady state during the experiment. Thus, the role of the PVB layer is to sustain a fixed concentration of chloride and create a bridge between the electrolyte inside and outside the membrane.

The proposed RE was later successfully incorporated into a fully-fledged, drop-casted commercial carbon fibre sweat sensor presenting a near-Nernstian response ($55.9 \pm 0.8 \text{ mV/log} [\text{Na}^+]$) in artificial sweat containing sodium levels between 10^{-3} M and 10^{-1} M [49], leading the scientific community to further develop the proposed scheme by taking advantage of DC simplicity or adapting the structure via screen printing. As a

result, when compared to a pseudo-reference electrode, the new RE scheme includes an additional layer, a reservoir, responsible for controlling the RE chloride concentrations and, as a result, ensuring a stable half-cell potential (Figure 3c).

3.1.2. Reference Electrodes: Ongoing Advances

Numerous proposals have adapted the RE structure in Figure 3c, introducing slight differences to optimize its electrochemical performance [38–45]. A summary of the drop-casted and screen-printed reference electrodes discussed is provided in Table 2 for a better comparison amongst them. The table includes performance and fabrication differences highlighted with their advantages and disadvantages and their suitability for certain applications.

Table 2. Summary of the REs proposed in the recent literature. Notation: AGTPB—silver tetraphenylborate, TBATPB—tetrabutylammonium tetraphenylborate, PVA—poly(vinyl acetate), PDMS—polydimethylsiloxane, SG—silicone gel, PVdF—poly(vinylidene difluoride), MM—methyl methacrylate, BM—butyl methacrylate, PBA—poly(butyl acrylate), NaTFPB—sodium tetrakis [3,5-bis(trifluoromethyl)phenyl] borate, TDMA—tridodecylmethylammoniumchloride.

Structure	Method	Advantages	Disadvantages	Ref.
Ag AgTPB PVC + TBATPB	SP, DC	Suitable structure for solid state and flexible REs. Remarkable lifetime and negligible potential drift towards various electrolytes even under mechanical stress.	Time/cost differences between the development of reservoir layers with hydrophilic or organic insoluble salts require further addressing.	[38]
Ag AgCl KCl + PVA PDMS	SP	PDMS junction suppresses electrolyte leaking, conferring potential stability over a month and ion insensitivity.	Electrolyte stability comes at the expense of long hydration times (30 min).	[39]
Ag AgCl KCl + PVA	DC	Stable Nernstian response even after five months over a wide pH range (1–10).	Crosslinked PVA increases hydration time. There are no assays regarding sensitivity to ions.	[40]
Ag AgCl KCl + PVB	IJP	Negligible potential drift under a wide range of pH and Cl [−] concentration ranges. Three-month stability.	PVB cocktail requires a mix of four solvents. A limited library of interferents has been evaluated.	[41]
Ag AgCl SG + PVdF	SP	Paper-based SPRE as an alternative to counterparts developed in plastic substrates.	Complicated structural assembly. Very limited lifetime and stability during measurements.	[42]
Ag AgCl PVC + NaTFPB	IJP, DC	Insensitive near-Nernstian potentiometric response to a wide range of pH (± 0.02 mV) and Cl [−] concentrations.	Requires extended conditioning and may suffer from unwanted structural changes in the process.	[50]
Ag AgCl KC + MM:BM	SP	Negligible potential drift (± 4 mV) under mechanical stress suitable for in-vivo pH sensing.	Not enough experimental data have been presented to define whether the proposed electrode is a pseudo-RE or an RE.	[43]
Ag AgCl KCl + PVA	DC	Negligible potential drift under light exposure and a wide range of pH. Successful integration into a miniaturized chip wearable device.	Considerable technical and cost requirements given the characteristics of the electrochemical device.	[44]
Ag AgCl PBA + NaTFPB:TDMA	SP	Polymeric and lipophilic salt reservoir confers low interference (9 mV) against a wide spectrum of anions.	Short lifetime and high potential drift under the presence of perchlorate ions.	[45]

As detailed in Table 2, the literature review indicates that the development of reference electrodes has gradually increased in both structural and functional sophistication. Starting with those electrodes that present a similar structure to the RE introduced in Figure 3c, Moya et al. [41] adapted the drop-casted RE proposed by Andrade et al. [48,49] via inkjet printing, obtaining a stable and reusable RE composed of Ag|AgCl|KCl + PVB. The electrode was produced by consecutive printing of several layers: a silver ink, which was further chlorinated with NaClO printing, and a reservoir/protection layer, obtained by printing a Cl[−] saturated polyvinyl butyral membrane (Figure 4A). It is pertinent to

note that, compared to the simplicity of the PVB cocktail used in DC, the reported PVB cocktail required a mix of four solvents (methanol, butanol, xylene, and diacetone alcohol) to successfully control both the inkjet printing and the drying processes. It has often been found that functional electrodes produced by drop casting can later be inkjet printed; however, the requirements of inks in terms of surface tension, viscosity, and drying require modifications to their formulation, such as mixes of solvents or the addition of additives [51]. Regarding its performance, the Ag | AgCl | KCl + PVB presented negligible potential drift under a wide range of pH (3–10) and Cl⁻ conditions (KCl, NaCl and CaCl₂) compared to a double junction reference electrode, in addition three-month stability. Additional sensitivity essays focused on ions suspected to be responsible for potential changes in the outer pH values could be considered a pending aspect.

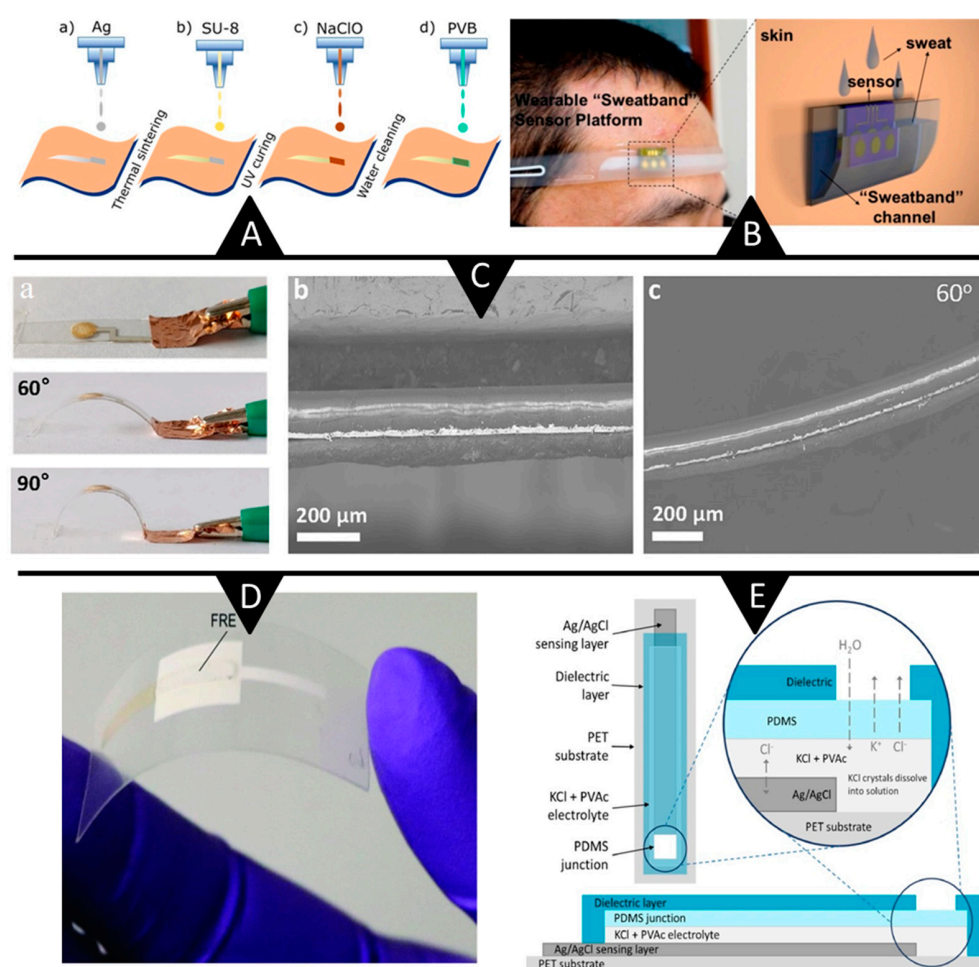


Figure 4. (A) Fabrication process of an IJPRED protected by a printable PVB-based membrane [41]. (B) Wearable sensor platform based on a solid-state ISE gold nanodendrite electrode and a Ag | AgCl | KCl + PVA membrane-coated RE [44]. (C) (a) Photograph of Ag/AgTPB/PVC-TBATPB under no bending and 60 and 90° bending. (b,c) Scanning electronic microscopy images of Ag/AgTPB/PVC-TBATPB flexible SCRE developed by Gan [38]. (D) Image of the as-obtained thick-film Ag | AgCl | KC + MM:BM SCRE reported by Manjakaal [43]. (E) Structure and composition of the SPRE proposed by Dawkins et al. [39]. Inset: ionic exchange pathways within the electrode and between the electrode and the analytes. (A) Reprinted with permission from [41]. Copyright (2019), American Chemical Society. (B) Reprinted with permission from [44]. Copyright (2017), American Chemical Society. (C) Reprinted with permission from [38]. Copyright (2022), American Chemical Society. (D) Reprinted with permission from [39]. Copyright (2018), WILEY-VCH Verlag GmbH & Co. KGaA, Weinheim. (E) Reprinted from [39], Copyright (2021), with permission from Elsevier.

Introducing slight differences to the formulation of the reservoir layer, Macedo et al. [40] and Bananezhad et al. [50] described the construction of a novel RE with exceptional long-term stability. In the former case, an RE was constructed by electrochemically coating a silver wire with AgCl in a 1 M KCl solution and further drop casting the KCl + PVA membrane. This initial construction scheme was found to undesirably leak Cl^- from the reservoir layer to the measurement solution, leading researchers to add a stage to the preparation process, consisting of a crosslinking step using ethylene glycol dimethacrylate (EGDMA). The obtained RE demonstrated a performance comparable to that of a commercial reference electrode, including a stable Nernstian response even after five months over a wide pH range (1–10), being a structural trade-off diminishing the Cl^- leak ratio by 30% against moderate to long hydration times due to the crosslinking process. Furthermore, the RE performance was compared to that of a commercial RE in electrochemical set-ups to determine pH, showing differences of less than 2% in complex samples, such as tap water, sea water, and coffee.

On the other hand, Bananezhad et al. [50] developed a flexible solid-state RE for which inkjet printing was used to fabricate the conductive path and silver patterns that were chemically transformed into the Ag|AgCl electrodes. The as-obtained electrode was further drop-casted with a membrane containing PVC, KCl, and NaTFPB. This IJPRE exhibited a near-Nernstian potentiometric response to a wide range of pH (3–10) and seven different electrolytes (NaNO_3 , KNO_3 , NaCl, NaF, CaCl_2 , KBr, and KCl) over a broad concentration range (10^{-6} to 10^{-1} M). Despite the aforementioned figures of merit and the reported four-week shelf life, the IJPRE presented resistive electrochemical behaviour, requiring up to 3 h to reach a stable potential without preconditioning. As a counterpart to the requirement of extended preconditioning in 1 M KCl, this process could cause unwanted changes in its porous arrangement, affecting the ion exchange on the membrane-solution boundary.

Alternatively, Manjakaal [43] developed an SPRE on a polyethylene terephthalate substrate, the reservoir of which consisted of KCl + MM:BM. The SPRE was sequentially prepared by alternating stages of printing and chlorination to obtain a reproducible layer of Ag|AgCl to which the reservoir layer was added later (Figure 4D). The reported results indicated that the produced RE exhibited negligible potential drift (± 4 mV) under mechanical stress (bending states between 3 mm and 7 mm). However, the lack of experimental data regarding potential stability outside of limited experimental conditions (NaCl, H_3PO_4) does not allow for dismissing the possibility that the RE is operating as a pseudo-RE.

Targeting another type of substrate for this sensing platform, Wang et al. [44] developed a wearable solid-state ISE and RE on a miniaturized chip using a gold nanodendrite (AuND) array electrode as the solid contact and a poly(vinyl acetate)/inorganic salt (PVA/KCl) membrane-coated RE. The Ag|AgCl|KCl + PVA RE was fabricated through the sequential drop-casting of a Ag|AgCl commercial ink, followed by a KCl + PVA composite (Figure 4B). Potentiometric results of the obtained RE indicated a lack of potential drift under light exposure, a wide range of pH, and different ions (Cl^- , NO_3^- , SO_4^{2-}) over a broad concentration range from 10^{-1} to 10^{-6} M. Additionally, on-body trials performed using a sweat headband indicated that the proposed sensor constitutes a reliable platform for Na^+ monitoring, requiring 20 min of pre-conditioning in 3 M KCl and standard calibration in a concentration range of 10^{-4} – 10^{-1} M to avoid initial potentially noisy signals.

While Komoda et al. [42] successfully fabricated a paper-based, planar-type RE using an Ag|AgCl commercial ink alongside a silica gel-poly(vinylidene difluoride) ink, the latter fulfilled the role of a hydrophilic liquid junction and electrolyte layer. The as-prepared Ag|AgCl|SG + PVdF SPRE presented a pseudo-Nernstian response in NH_4Cl , KNO_3 , NaHCO_3 , and K_2CO_3 solutions, reaching a stable potential within 5 min. Unfortunately, due to either computer-aided design requirements or limited results regarding lifetime and stability, there is a lack of recent proposals continuing this line of work.

After this first instance in the literature review, the abundance of reports of REs based on successive Ag|AgCl and polymer/electrolyte composite layers may indicate either a solved case or a lack of suitable experimental alternatives. However, the works of

Alva et al. [45], Gan et al. [38] and Dawkins et al. [39] indicate that there are other viable strategies outside introducing slight changes to the polymeric composition of the reservoir layer to enhance the analytical figures of merit of an RE. Alva et al. aimed to replace the standard composition of the reservoir layer by screen-printing an ion-permeable membrane consisting of a photocurable acrylic ink that contained immobilized lipophilic Na^+ and Cl^- salts (NaTFPB and TDMA-Cl). By optimizing the ratio between the two salts (1:1), the authors reported that the RE presented low and time-dependent potential drift towards KCl, ranging from 10^{-6} M to 1 M, changing the potential drift value from 1 to 10 mV after 7 h. This phenomenon was attributed to an uneven charge distribution inside the reservoir layer, an unwanted by-product of using lipophilic salts. Despite the reported issues, the SPRE exhibited remarkable insensitivity towards NO_3^- , Br^- , and SO_4^{2-} within a concentration range of 0.1 M to 10^{-8} M.

Gan et al. [38] focused their efforts on minimizing the risk of electrolyte leakage, replacing a hydrophilic electrolyte in the reservoir layer polymer matrix with a silver organic insoluble salt (AgTPB). The SPRE consisted of an Ag | AgTPB substrate and a plasticized PVC membrane containing TBATPB, another hydrophobic organic salt ($\sim 0.26 \mu\text{M}$ in water), to further prevent leaking (Figure 4C). Functionally, the proposed electrode worked following the basic principle of a standard Ag | AgCl-based SPRE, in which the fixed potential is given as a product of an electron-coupled ion transfer reaction mechanism that occurs at the Ag | AgTPB and AgTPB | PVC + TBATPB interfaces ($\text{AgTPB (s)} + e^- \rightleftharpoons \text{Ag (s)} + \text{TPB}^- (\text{PVC})$).

The reported results indicate that the Ag | AgTPB SPRE potential stability was tested against various electrolyte solutions (~ 4.8 mV), light (~ 0.5 mV), gas (N_2 , O_2 and CO_2 , ~ 5 mV), and redox interference ($\text{K}_3[\text{Fe}(\text{CN})_6]/\text{K}_4[\text{Fe}(\text{CN})_6]$, ~ 5 mV), showing negligible potential drift as indicated respectively in parentheses. As for potential responses to electrolytes (NaCl, LiCl, KCl, NH_4Cl and KNO_3) within a concentration range from 10^{-5} to 10^{-1} M, the electrodes showed potential variations of $4.6 \text{ mV} \pm 0.8 \text{ mV}$ and $10.6 \text{ mV} \pm 1.8 \text{ mV}$, respectively, with the significant drift increasing under high ionic strength, adjudicated to the unstable phase boundary potential between PVC | TBATPB and water interfaces due to differences in ion distribution in the two immiscible phases. Furthermore, the SPRE, alongside a mini-potentiometer and a mobile battery, was tested as a wearable sweat sensor, presenting a Nernstian response towards Cl^- , allowing for high accuracy Cl^- determinations, with relative error of 7.0% compared to other standardized methods, such as ion chromatography.

Finally, Dawkins et al. [39] prioritized solving Cl^- leaking issues from the reservoir spectrum, adding an additional layer to the traditional structure of SPREs. In this case, SCREs were fabricated on PET substrates printing sequential layers containing an Ag | AgCl commercial ink, an electrolyte composite containing KCl and PVA, and a PDMS membrane (Figure 4E). The latter, due to balanced permeability and hydrophobicity, acts as a liquid junction and dielectric protective coating able to increase the RE lifetime and stability through electrolyte retention. The previous statement was supported via a thorough report containing a structural characterization via SEM micrographs and EDS scans for the analysis of the electroanalytical figures of merit of the SCRE.

Results concerning the potential stability and lifetime through OCP measurements in 0.1 M K_2SO_4 indicated low drift rates (0.25–0.05 mV/day) at up to three months being observed only when an additional PDMS layer was present, while Ag | AgCl | KCl + PVA SCRE failed to present a consistent Nernstian response owing to KCl particle loss and compositional changes. Moreover, the disclosed SCRE insensitivity to various interferents, such as halide/alkali ion species (up to 5 mV of potential drift), and a wide range of pH conditions ($+0.29 \text{ mV/pH}$), further highlights, compared to the recent literature, the effectiveness of the PDMS layer. Withal et al., as well as Macedo et al. [40], proposed an SPRE used in combination with a commercial pH probe to determine the pH of complex samples, such as tap water, creek water, and coffee, showing good agreement with a commercial pH meter. However, it required long hydration times that could reach up to 90 min depending on the sample characteristics, an expected disadvantage attributed to the

addition of a PDMS layer that should be weighed, depending on the sensing requirements, against improvements in potential stability and lifetime.

3.1.3. Reference Electrodes: Lingering Challenges

As presented in this section, considerable work has been performed regarding the development of reference electrodes. Regarding the aforementioned publications, many of them came both functionally and structurally as close as needed to replace the conventional glass silver/silver chloride gel RE. Moreover, a small number have managed to make the leap from proof of concept to application in context.

However, there is still room for development in this field if we consider the current state of the art in three interconnected requirements. The first one refers to the reduction in costs linked to the manufacturing process, considering that works up to 2021 continued to ground within their novel aspects the presentation of a low-cost experimental design. According to recent literature [34], alternatives to the macroscale conventional RE should be at least an order of magnitude cheaper, while presenting remarkable potential stability and an extended lifetime. The latter constitute the two additional requirements and can be further improved, reducing the overall costs in the process.

From the prior works, it is possible to state that, from the chloride concentration on the reservoir layer to the composition and thickness of a polymeric layer to reduce ion leakage, many structural elements have significant effects on the RE's potential stability and lifetime. Regarding potential stability, Sophocleous [34] presented extensive research regarding the influence of the KCl to polymer weight ratios on the reservoir layer of REs, identifying significant differences in both base potential at physiological pH and potential drift towards chloride concentrations. Despite indicating that the optimization of said layer is a crucial aspect, not all recent proposals that used diverse polymeric reservoirs performed this needed characterization. The proposed layer optimization study is even more relevant considering the recent alternatives to hydrophilic reservoirs by the addition of insoluble organic salts. Furthermore, given the reported results after chlorination of a silver layer [41], researchers may even evaluate intervening in previous stages of its assembly, such as studying the possible effects over potential drift of replacing the use of highly reproducible commercial Ag/AgCl inks with the controlled synthesis of composites such as Ag@AgCl [52], reducing overall costs.

From a durability standpoint, while optimizing conditions for the reservoir layer can also enhance the RE lifetime, the presence of an additional permeable and hydrophobic epoxy-based junction layer on top of the RE was reported to dramatically increase its lifetime [39]. Interestingly, this assembly proposal with an additional layer has been previously described as a suitable alternative for RE development [34,35], but to date, a majority of the reported reference electrodes have adhered to the structure proposed in Figure 3b.

In closing, it is important to emphasize that the alternatives proposed for the future development of RE could present a trade-off with other functional characteristics, such as hydration times, which should be evaluated considering the requirements of the targeted field of application. For instance, some applications resolved through disposable sensing platforms may require an RE with high selectivity and short hydration times instead of long-term stability. Therefore, considering the imbalance between proof of concept and field-applied works, future RE structures should be designed from square one to meet the requirements of a specific application, instead of prioritizing the development of an RE that excels in all functional domains.

3.2. Ion-Selective Electrodes

Ionophore-based ion-selective electrodes (ISEs) are widely used for the determination of ion activity in applications employed in fields such as environmental monitoring, life science, process control, and, in particular, routine clinical analyses. These ISEs deliver long-term stable potentials, and their electrode-to-electrode reproducibility is excellent, but

the miniaturization is not straightforward. Therefore, much effort has been devoted in past years to the development of solid-contact ISEs.

3.2.1. ISEs Structural Overview

Solid-contact ISEs are comprised of an electric contact, an ion-to-electron transducer, and a selective membrane that only allows the diffusion of the target ion to be sensed.

Regarding the most targeted ions in sweat, sodium and potassium, the component of the membranes has the following components: a polymer, a plasticizer, a counterion to the target ion, and an ionophore. The polymer provides a hydrophobic matrix with a low glass transition temperature, forming a stable surface and providing mobility of organic salts and sufficient electric conductivity of the membrane. The plasticizer decreases the glass transition temperature, increasing therefore the ion mobility and acting as a solvent for ionophores, preventing their phase separation. Then, the counterion provides ionic sites for the target ion, and it is usually a hydrophobic molecule that remains in the hydrophobic polymer matrix, preventing its release into the medium. Finally, the function of the ionophore is to complex the target ion, increasing its solubility in the membrane [53].

For other analytes, e.g., hydrogen ions, there are electrodes in which the sensitive component is the ion-to-electron transducer, such as in the case of polyaniline (PANI) [54], or oxides [55].

3.2.2. ISEs: Ongoing Advances

In recent years, much research has been directed towards the development of novel ion-to-electron transducers, aiming to increase the sensitivity, by either improving conductivity or by increasing the surface area on which the selective membrane is applied. Additionally, there has been much work in the development of conductive substrates to improve integration into flexible or small devices, such as textiles, wearables, or microfluidic devices. A collection of some of the latest reported ISEs is presented in Table 3.

Table 3. Summary of the ISEs proposed in the recent literature. Notation: LOD—limit of detection, LR—linear range, PET—polyethylene terephthalate, PVC—polyvinylchloride, KTPFB—potassium tetrakis(pentafluorophenyl)borate, DOS—dioctyl sebacate, KTCIPB—potassium tetrakis(4-chlorophenyl)borate, NiCAT—nickel triphenylene-fused metal catecholate, NaTFPB—sodium tetrakis[3,5-bis(trifluoromethyl)phenyl] borate, NaBARF—sodium tetrakis[3,5-bis(trifluoromethyl)phenyl]borate, NPOE—nitrophenyl octyl ether, PANI—polyaniline, PEDOT:PSS—poly(3,4-ethylenedioxythiophene) polystyrene sulfonate.

Analyte	Substrate	Ion-To-Electron Transducer	Ion-Sensitive Membrane	Figures of Merit	Ref.
K ⁺	Commercial conductive ink printed on PET	Mix: β -cyclodextrin and rGO (pH-sensitive)	K ⁺ : valinomycin, KTPFB, PVC, DOS	pH: sensitivity = 54 mV/dec LOD = pH 10 K ⁺ : sensitivity = 56 mV/dec LOD = 10 ^{-6.2}	[56]
K ⁺	Stencil-patterned carbon electrode on PET, carbon black-modified		K ⁺ : valinomycin, KTCIPB, PVC, DOS	K ⁺ : sensitivity = 56.1 mV/dec LOD = 10 ⁻⁵ M LR = 10 ⁻⁴ to 10 ⁻¹ M	[57]
Na ⁺	CNT fibres on an elastic band	NiCAT coated with Nafion	Na ⁺ : sodium ionophore X, NaTFPB, PVC, DOS	Na ⁺ : sensitivity = 58.7 mV/dec LOD = 10 ⁻⁶ M LR = 10 ⁻⁵ to 10 ⁻¹ M	[58]
Na ⁺	Gold electrodes on PET	Nafion-covered porous 3D graphene	Na ⁺ : Na ionophore X, NaBARF, PVC, NPOE	Na ⁺ : sensitivity = 65.1 mV/dec	[59]
Na ⁺ and K ⁺	Screen-printed commercial electrode		Crown-ether-functionalized graphene quantum dots	Na ⁺ and K ⁺ : 42 mV/dec, but no selectivity	[60]

Table 3. Cont.

Analyte	Substrate	Ion-To-Electron Transducer	Ion-Sensitive Membrane	Figures of Merit	Ref.
H ⁺	RGO dry-spun fibres	Ferrocene	pH: 4-nonadecylpyridine, PVC	pH: 55 mV/dec	[61]
Cl ⁻	Screen-printed carbon electrodes	PANI, acrylic binder		pH: sensitivity = 66 mV/dec	[54]
H ⁺ , Na ⁺ and K ⁺	Laser-induced-graphene on Kapton	pH: PANI Na ⁺ and K ⁺ : PEDOT:PSS	Na ⁺ : Na ionophore X, NaTFPB, PVC, DOS K ⁺ : valynomicin, KTCIPB, PVC, DOS	pH: sensitivity = 51.5 mV/dec Na ⁺ : sensitivity = 45.4 mV/dec K ⁺ : sensitivity = 43.3 mV/dec	[62]
Na ⁺	Leather	Graphite-Na _{0.44} MnO ₂ mix		Na ⁺ : sensitivity = 58 mV/dec	[63]

Among the works presented in Table 3, there is a group of sensors, the electrodes of which are manufactured applying layers on a substrate, such as PET [56,57,59], Kapton [62], and even leather [63]. These substrates provide flexibility, although the integrity and functionality of the sensors must be checked during or after the bending to assure flexibility. In the other group of sensors, the electrodes are manufactured using conductive fibres as a substrate, e.g., carbon nanotube fibre (CNTF) [58] or RGO fibre [61].

Even though there are various combinations of membranes, transducers, and conductive electrodes, most of the sensitivities reported are around the Nernstian behaviour (59 mV/dec).

The simplest electrode to measure potassium is the one presented by Henry et al. [57], comprising a carbon electrode applied with a stencil on PET and then covered by different cocktails of valynomicin, PVC, plasticizers (dioctyl sebacate (DOS), or nitrophenyl octyl ether (NPOE)) and additives (potassium tetrakis(4-chlorophenyl)borate (KTCIPB) or sodium tetrakis[3,5-bis(trifluoromethyl)phenyl]borate (NaTFPB)) in THF. This work compares the addition of carbon black prior to the sensitive membrane, showing that this approach increases the surface area of the electrode and hence its sensitivity. For the membrane cocktail with the highest sensitivity (56 mV/dec), the standard deviation for five sensors is about 1.25%. This work also shows that the limit of detection (LOD) for potassium is as low as 10⁻⁵ M with a linear range between 10⁻⁴ and 10^{-1.1} M, compatible with normal values in human sweat.

Subsequently, Gao [59] presented a sensor for sodium in sweat. To enhance the sensitivity, they synthesized 3D porous graphene by chemical vapour deposition (CVD). This graphene has a gradient-like porosity that increased dramatically the electrochemically active surface area. Then, this carbonous material was deposited on a gold electrode, and a sodium selective ionophore solution was casted on top of that. Using this approach, they claimed to achieve the highest sensitivity for sodium ions, 65.1 mV/dec.

Another carbon-based potassium sensor was created by Wu [64], without an ion-electron transducer. In this work, the conductive electrode was of porous carbon resulting from laser engraving of an adhesive layer of PI. On top of this layer, a selective membrane of valynomicin, PVC, sodium tetraphenylborate (NaTPB), and DOS was casted. This work is interesting because they evaluated the effects of different bending angles, up to 60°, and tested the performance after 8000 bending cycles. The sensor experienced no significant reduction in sensitivity (58.1 mV/dec before bending and 57.4 mV/dec afterwards). A drawback of this sensor is that the calibration curve is displaced when the sensor is bent, so the measurement must be performed at a constant angle to be reliable.

Another group of sensors involves the use of ion-electron transducers applied on top of the conductive electrode. Sun et al. [56] worked on a flexible sensor in which a β-cyclodextrin functionalized graphene (β-CD/RGO) was printed on a conductive layer with a commercial ink on PET. The combination of β-CD with the graphene provides many oxygen functional groups, and it possess good capacitance, giving this material

pH sensitivity ranging from 48 mV at a 0° bending angle to 51 mV/dec at a 90° bending angle. This material also acts as ion-electron transducer, which was tested by applying a potassium selective membrane, with a response of 55 mV/dec regardless of a bending angle between 0° and 90°. These sensors were used to build a wearable device for on-body sweat analysis. The linear response had no significant fluctuations before or after the test, indicating that the on-body analysis data were reliable.

Conductive polymers were used as ion-electron transducers for several analytes. Moreover, Lin et al. [62] proposed a platform using laser-induced graphene electrodes covered with PEDOT:PSS and ion-selective membranes to measure Na⁺ and K⁺ and PANI to measure pH. In this work, they built a multiplexed device for real time sweat analysis with Bluetooth communication using an app in a smartphone. The sensitivities achieved for pH, Na⁺, and K⁺ were 51.5 mV/dec, 45.4 mV/dec, and 43.3 mV/dec, respectively. The sensors showed no apparent change in the potential response upon bending, and they were tested by a subject on a stationary bicycle for almost 2 h.

PANI was also used by Bilbao et al. [54] to measure the pH of synthetic sweat. This work presents a scalable process to manufacture sensors via screen-printing and inkjet-printing techniques, and the PANI is mixed with acrylic binders to increase the wear resistance. While the authors did not perform on-body testing, the adhesion and friction resistance were measured and compared to electrodeposited PANI, showing that the addition of binder increased the resistance without compromising high sensitivity (62 mV/dec) and selectivity.

Khoshshafar [63] presented a sensor for sodium detection using a mix of graphite and Na_{0.44}MnO₂. To achieve flexibility at low cost, this paste was applied on a leather band. Na_{0.44}MnO₂ was used because it has a crystalline structure that allows for Na⁺ accommodation and provides sensitivity. Graphite is a conductor, and PVDF is used as a binder, with no effect on the potentiometric behaviour. This sensor has sensitivity of 58 mV/dec, and the authors tested it both off-body and on-body using a headband. This band uses a hydrophobic coating to direct the collected sweat towards the sensing area.

A different approach for sensor manufacturing and integration consists of building the sensor on a conductive fibre. In this regard, Omenetto et al. [61] used dry-spun fibres of pure reduced graphene oxide (RGO) as a substrate. They reported the functionalization of these fibres with ferrocene, which increased the ion-electron transduction, enhancing the sensitivity. The fibres were functionalized with a membrane consisting of PVC and a pH ionophore, 4-nonadecylpyridine, applied by spray coating. The sensitivity increased from 48.3 mV/dec without ferrocene to 55.0 mV/dec when it was present. The variation in sensitivity from sensor to sensor was low for both types of sensors, suggesting that fibre fabrication and functionalization produced sensors with high reproducibility.

Finally, Wang et al. [58] presented another fibre-based sensor constructed of carbon nanotube fibre (CNTF) and a metal-organic framework (MOF), as shown in Figure 5. Vertically aligned nanowires of nickel triphenylene-fused metal catecholate (NiCAT) were grown in situ through a one-step hydrothermal reaction. The nanowires were coated with a thin layer of Nafion and then covered with an ion-selective membrane. In this work, a sodium-selective membrane was used, providing sensitivity of 58.7 mV/dec. The combination of Nafion and NiCAT nanowires yielded a well-defined capacitive behaviour for efficient ion-electron transduction. Additionally, the Nafion prevented the accumulation of water between the MOF and the ion-selective membrane.

3.2.3. Ion-Selective Electrodes: Lingering Challenges

According to the reviewed literature, large numbers of works have shown multiple sensors with proven abilities to measure ions in sweat with on-body testing or at least constructed of flexible substrates that ease integration into wearable devices.

A next step in research and development could be directed towards the life cycle of these devices, aiming for long-term usability. Some aspects that could be worked on are wear resistance and endurance studies when sensors are exposed for long periods of time to

sweat or washing solutions. While these aspects are considered in the short-term on-body tests, it could be interesting to perform a more systematic analysis.

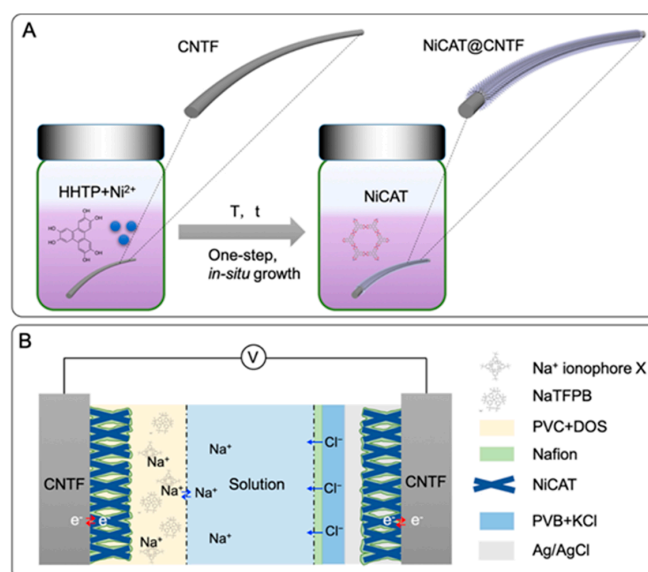


Figure 5. Schematic illustrations of the fabrication and structure of the NiCAT@CNTF-based ISE and RE [58]. (A) One-step in-situ growth of NiCAT on CNTF in a liquid containing the organic linker of HHTP and Ni(II). (B) Schematic profile of NiCAT@CNTF-based ISE and RE in an electrochemical cell. Reprinted from Ref. [58]. Copyright (2022), with permission from Elsevier.

4. Sensing Metabolites in Sweat with Amperometric Enzyme Electrodes

Amperometric enzymatic biosensors are usually employed to detect small organic molecules, such as metabolites, in biological fluids, such as sweat, tears, exhaled breath, and saliva, for diagnosis, treatment, control of medical conditions, and fitness applications [65]. A biosensor consists of three main components: a bioreceptor, a transducer, and a signal processor [66]. The bioreceptor is composed of a biological recognition element (an enzyme, an antibody, a protein receptor, DNA, or whole cells) that recognizes the target analyte. The transducer converts the recognition event into a measurable signal (electrical, optical, thermal, electrochemical, or piezoelectric). Biosensors aiming for the determination of metabolite levels in sweat usually employ an enzyme that specifically recognises it and catalyse a reaction, the rate of which can be effectively followed by amperometric or voltammetric techniques. Enzyme electrodes have been used to detect glucose [67], lactate [24,65,68,69], ethanol [29], and levodopa [70], among other substances. Table 4 summarizes the metabolites detected by amperometric sweat sensors, their physiological concentrations, enzyme types, electrode characteristics, detection limits, sensitivity, linear ranges, operation, storage stability, and related diseases.

Redox mediators are utilized to transfer electrons between the enzyme and the electrode. Mediators can be immobilized onto the surface of the transducer, together with the enzyme. Prussian blue is a widely used redox mediator in sweat sensors for the detection of various analytes, including glucose [33], lactate [68], and ethanol [29]. However, direct electron transfer is also possible between the active side of the enzyme and the transducer without the need for a mediator [71]. Mediator-free sweat sensors have also been used in sensors to determine analytes, such as glucose [72] and ascorbic acid [73]. Regarding the construction of the electrodes, similar approaches to those used for potentiometric measurements have been followed, with the extensive use of screen-printed electrodes modified by drop casting or inkjet printing. Fully inkjet-printed biosensors are particularly adequate for sweat biosensing since they can be printed on flexible substrate, although the integration with the electronic processing circuit still presents some challenges (see Section 6 on electronic instrumentation).

Table 4. Enzyme electrode biosensors for sweat analysis. References: ACA: anisotropic conductive adhesive; AOx: alcohol oxidase; HRP: horseradish peroxidase; LOx: lactate oxidase; MWCNTs: carboxy-functionalized multiwalled carbon nanotubes; PB: Prussian blue; PDMS: polydimethylsiloxane; PP: polypropylene; PPD: poly-m-phenylenediamine; SPCE: screen-printed carbon electrodes; SPPB: screen-printed Prussian blue conductive carbon; 3D-PMED: 3D paper-based microfluidic electrochemical integrated device; NA: not available.

Analyte	Relative Content in Sweat	Enzyme	Redox Mediator	Electrode Material	Electrode Substrate	Linear Range; Sensitivity	Detection Limit	Sample	Data Acquisition	Response Time	Operation Stability; Storage Stability	Disease Correlation	Ref.
Glucose	10–200 mM [2]	GOx	Prussian Blue	CNT fiber electrode (CE, WE), Ag/AgCl fibre (RE)	Fabric	0–200 μM ; 2.15 nA μm^{-1}	NA	Sweat after 10 min of exercise	Bluetooth	30 s	NA	Diabetes	[67]
		GOx	Prussian Blue	Blue/graphite ink (WE), SP graphite ink (CE) Ag/AgCl (RE)	Paper (3D-PMED)	0–1.9 mM; 35.7 mA mM^{-1} cm^{-2}	5 mM	Sweat from forehead during cycling	Wires	60 s	NA		[33]
		GOx	Mediator-free	PPD/PtNP/Au/ACA (WE), Ag/AgCl (RE)	ACA	0–600 μM ; 15.1 $\mu\text{A}/\text{mMcm}^{-2}$	0.9 μM	Iontophoresis	Bluetooth	60 s	10-h; NA		[72]
Lactate	5–20 mM [2]	LOx	1,2-naphthoquinone	Carbon/GMgOC (WE), carbon (CE), and Ag/AgCl (RE)	PDMS	0–50 mM (36.2 μA mM^{-1} cm^{-2})	0.3 mM	Artificial sweat	Wires and sticker-based connector	2–6 min	NA	Cystic fibrosis, stress ischemia, lactic acidosis	[69]
		LOx, HRP	Os-complex	graphite paste (CE, WE), and WE modified with MWCNTs	PP	0–25 mM (0.74 μA mM^{-1})	0.04 mM	Sweat from forehead during cycling	Wires	60 s	Intervals during 6-h; NA		[24]
		LOx	Prussian Blue	Ag/AgCl (RE), SPCE (CE)	Flexible substrate	1–222 μM (40.6 μA mM^{-1} cm^{-2}) 0.222–25 mM (1.9 μA mM^{-1} cm^{-2})	0.8 μM	Sweat from forehead while walking	Bluetooth	100 s	Sensitivity remained 88.3% after multiple use in 20 days; NA		[68]

Table 4. Cont.

Analyte	Relative Content in Sweat	Enzyme	Redox Mediator	Electrode Material	Electrode Substrate	Linear Range; Sensitivity	Detection Limit	Sample	Data Acquisition	Response Time	Operation Stability; Storage Stability	Disease Correlation	Ref.
Ethanol	2–30 mM	AOx	Prussian Blue	SPPB conducting carbon, AOx, chitosan (WE), SPPB conducting carbon (CE), Ag/AgCl (RE)	Tattoo	$0\text{--}40 \times 10^{-3}$ M; NA	NA	Sweat by 5-min iontophoresis	Bluetooth	60 s	At least 10 repetitions; NA	Alcoholism, hepatitis B, diabetes, drunk driving	[29]
Ascorbic acid	10–50 mM [2]	Ascorbate oxidase	Mediator-free	Ag/AgCl (RE), SPCE (CE), and Rh-SPCE (WE)	Tattoo polyurethane	0–1000 μ M; NA	NA	Sweat stimulation of forearm	Wires	60 s	2 h after ingesting vitamin C; NA	Tumours, cancer, kidney disease, thrombosis, stones	[73]
Levodopa	Dose dependent	Tyrosinase	Thionine acetate	Au nano dendrites on Au/Cr tyrosinase (WE), Ag/AgCl (RE), and Au (CE)	PET	1–1000 mM; 1.7 nAmM^{-1}	1 μ M	Sweat by 5-min iontophoresis	Wires	200 s	NA	Parkinson's disease monitoring and optimization	[70]

Several drawbacks, such as enzyme immobilization, high cost, low operation stability due the changes in pH, temperature, and humidity dependence, are currently the main issues to be resolved, especially for the development of continuous monitoring sensors. Hence, researchers are also currently working to develop high performance nonenzymatic sensors [74]. The current challenges presented by amperometric sweat sensors are related to the operational stability and long-term stability of functional materials, the effect of pH variations in sweat on the sensing device, signal fluctuation caused by the bending of wearable sensors, chemical interference, and the use of suitable materials in continuous monitoring and sampling [4].

4.1. Immobilization Strategies in the Development of Enzymatic Biosensors

Enzymes that are immobilized onto solid substrates exhibit improved resistance to harsh conditions, such as low or high pH, temperature, and dryness, both during their use in biosensors and during storage, and they also have enhanced stability over time [74]. Various immobilization strategies are usually employed on sweat sensors.

Figure 6 summarizes the main strategies used for bioreceptor immobilization [51]: adsorption, covalent immobilization, and entrapment. In some cases, enzyme immobilization protocols are based on the combination of several immobilization methods. Physisorption can be attained by simple exposure of the electrode to a bioreceptor suspension; however, the interaction may be weak and unspecific, and usually other means are preferred for the immobilization of molecular bioreceptors based on covalent bonds or highly specific and strong interactions.

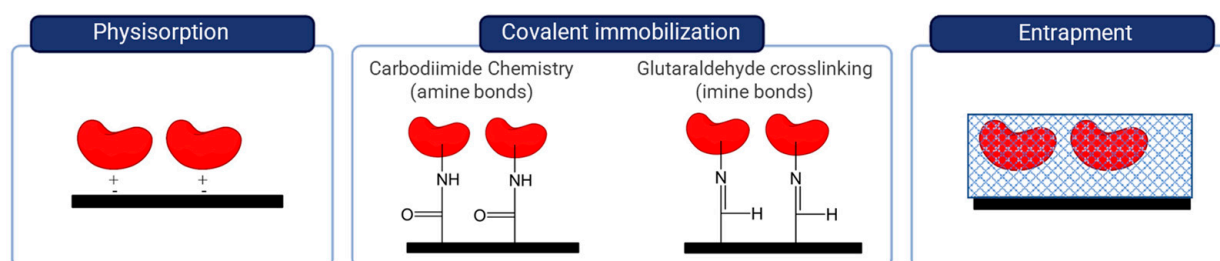


Figure 6. Schematic representation of the most common methods used to immobilize bioreceptors in the development of sweat biosensors. Physisorption relies on intermolecular interactions between the bioreceptor (red) and the electrode (black). Most common methods for covalent immobilization rely on the formation of amide or imine bonds. Bioreceptors can be also entrapped by encapsulation within a hydrogel (light blue).

Enzyme physisorption onto solid substrates represents the easiest method of physical immobilization. Physical adsorption consists of the simple deposition of an enzyme onto a surface and its attachment through weak bonds. The adsorption mechanisms are based on weak bonds, such as Van der Waal forces and electrostatic and/or hydrophobic interactions. This technique may not involve any functionalization of the substrate and generally does not have a significant effect on the enzyme activity. Nevertheless, physisorption immobilization may have poor operational and storage stability because it can be affected by fluctuations in temperature, pH, and ionic strength, leading to the desorption of loosely bound enzymes.

Enzymes can also be electrostatically immobilized onto charged surfaces, taking advantage of the intrinsic surface charge of the material or coating the electrode with a polyelectrolyte with a charge opposite to that of the enzyme at a certain pH. Layer-by-layer immobilization based on electrostatic adsorption is widely used in the development of enzymatic biosensors. For example, wearable fabrics for real-time glucose monitoring were developed using sensing fibres of CNT with Prussian blue as a redox mediator. Then, the CNT electrode was coated with chitosan, and glucose oxidase (GOx) was immobilized by electrostatic interactions [67]. Cao et al. developed a paper-based microfluidic electro-

chemical device for glucose detection, coating the carbon electrode with a layer-by-layer of Nafion/chitosan/GOx/chitosan/Nafion [33]. This repeatable number of layers provides a strategy for the rational design of the properties of immobilized films; for instance, a Nafion layer is critical to removing interferences present in sweat. Kim et al. [29] developed a temporary tattoo for simultaneous monitoring of ethanol and glucose. In this work, they used chitosan to immobilize alcohol oxidase (AOx) and glucose oxidase onto screen-printed Prussian blue carbon electrodes.

Covalent coupling of enzymes to different substrates is a popular chemical immobilization method. The enzymes are bound to the surface through functional groups, which are not essential for their catalytic activity. Covalent immobilization is more reliable and specific than adsorption and provides more stability to the recognition element. The binding of the enzymes to the solid support is generally conducted by initial activation of the surface using multifunctional reagents, such as carbodiimide [75] or crosslinking with glutaraldehyde [76], followed by enzyme coupling to the activated substrate with the removal of excess and unbound biomolecules.

In the development of sweat sensors, various authors have chosen covalent coupling as an immobilization method. Shitanda et al. [69] developed a lactate sensing system using a screen-printed sensor based on graft-polymerized MgO-templated carbon, onto which lactate oxidase was covalently bound. Sempionato et al. [73] developed flexible printable tattoo electrodes for monitoring changes in the vitamin C level in sweat, in which the enzyme ascorbate oxidase was immobilized on the Rh-metalized carbon electrode via glutaraldehyde crosslinking. Glutaraldehyde has also been used to immobilize tyrosinase, an enzyme that facilitates the electrochemical oxidation of levodopa excreted in sweat [70]. Monitoring and optimization of levodopa dosage are critical in patients with Parkinson's disease.

Entrapment is a method of choice to immobilize enzymes in three-dimensional matrices, such as electropolymerized films, amphiphilic networks composed of polydimethylsiloxane (PDMS), photopolymers, silica gel, polysaccharides, or carbon pastes [77]. In these cases, enzymes, mediators, and additives can be simultaneously deposited on the same sensing layer. There is no modification of the bioreceptor, so the activity of the enzyme is preserved during the immobilization process. Biosensors based on physically entrapped enzymes are often characterized by increased operational and storage stability. However, limitations such as leaching of the bioreceptor and possible diffusion barriers can restrict the performance of the systems. Zhang et al. [24] developed an enzymatic biosensor for eyeglasses aimed at the determination of lactate in human sweat during physical exercise. Lactate oxidase (LOx) was immobilized on the working electrode surface by electropolymeric entrapment in a poly(phenylenediamine) (PPD) film.

Finally, it must be noted that the type of immobilization method affects the activity and stability of enzymatic biosensors, a subject treated in the next section.

4.2. Stability of Enzymatic Biosensors

Enzymes have been widely used bioreceptor molecules in biosensor applications [78]. Enzymes are able to recognize a specific substrate (or a class of substrates) and, therefore, are able to catalyse only a specific chemical reaction [79]. Electrochemical enzyme-based sensors are advantageous in several ways because they include the high specificity of the enzyme, as well as the sensitivity of electrochemical transducers. In these sensors the enzyme is immobilized on the electrode surface. The enzyme should be immobilized in the active form, and the activity must be preserved without reduction in the specificity for the analyte. It is known that immobilized enzymes frequently exhibit more stability than native enzymes [80]. However, the immobilization of an enzyme (or other protein) does not guarantee the stabilization of the enzyme structure. Stability generally results from the molecular rigidification introduced by the attachment of the protein molecule onto a solid support, with the concomitant creation of a protected microenvironment [81]. Factors such as accuracy of measurements, reproducibility, and operational lifetimes are drastically

influenced by enzyme stability, even more so in long-term application. Since the analytical performance of a biosensor is strongly affected by the immobilization process, intensive efforts have been undertaken to develop successful immobilization strategies to assure greater sensitivity and stability of biosensors [77]. Enzymes are sensitive to changes in pH, ionic strength, chaotropic agents, among other changes in the reaction medium, such as the presence of polymers, polysaccharides, surfactants, etc. [82]. Moreover, changes in the macroenvironment during any process could affect the enzyme stability involving cooling, freezing, or desiccation. Despite this fact, enzyme stability is the main challenge when achieving viable biosensors because it affects the shelf life and the operational stability of the sensor, amongst other variables. The enzyme stability has to be maintained or preferably increased to ensure the stability of the biosensor in terms of reusability and long term storage [83]. To preserve the enzyme activity is essential to obtaining a high response signal, principally in sensors for continuous monitoring.

Most of the biological responses converted by sensors require at least one to two years of storage stability, known as shelf stability, whereas operational stability depends on the type of biosensor. Operational stability varies from several minutes to several months [84].

Wearable sensors incorporate one or several inner or outer layers, in addition to the reacting layer or membrane. These layers or membranes serve three important functions: a protective barrier, a diffusional outer barrier for the substrate, and biocompatibility [84].

In past years, several authors have worked to improve the enzyme stabilization in wearable sweat sensors. Motosuke et al. [69] developed a microfluidic lactate-sensing system for the continuous monitoring of sweat lactate. The screen-printed sensor based on graft-polymerized MgO-templated mesoporous carbon (GMgOC) had the enzyme lactate oxidase and the redox mediator 1,2-naphthoquinone immobilized. The authors developed carbon materials with controlled pore sizes (with a diameter of approx. 100 nm) using MgO as a template. Then, the MgOC surface was modified with glycidyl methacrylate, and the enzyme was covalently bound to the graft-polymerized MgO-templated carbon via GMA polymers through epoxy groups that reacted with the amine groups of the enzyme. The large surface area of mesoporous carbon and the covalent binding of the enzyme translated into high response currents. To improve the stability of the sensor, they added sucrose, catalase, and PEGDGE. Sugar addition enhanced the thermostability of the enzyme. The sucrose stabilized the enzyme structure, thus extending the storage stability. Catalase increased the operational stability of oxidase-based sensors by deactivating the hydrogen peroxide produced by the oxidase when oxygen was used as the electron acceptor. Catalase was applied on the electrode, either together with LOx or in a separate subsequent step. Finally, the cross-linker PEGDGE enhanced the immobilization efficiency of LOx and catalase.

Particularly for sweat lactate monitoring, there are other parameters that affect the enzyme stability, such as the substrate concentration and sweat pH variations. The enzyme lactate oxidase (LOx) immobilized onto electrodes exhibited stronger substrate inhibition, resulting in the formation of large and inactive LOx aggregates. Cunha-Silva et al. [85] observed these phenomena with LOx crosslinking on modified screen-printed electrodes. In the lactate range from 4 to 50 mM, the biosensors showed a decrease in current signal due to a substrate inhibition process. In addition, the authors found that the substrate additions resulted in slightly acidic supporting electrolytes, generated by the dissociation of lactic acid in lactate and protons (pK_a 3.86). The change in the pH affected the crosslinked LOx activity, giving a place to lower rates of substrate catalysis. They solved this problem using concentrations greater than 0.5 M of phosphate buffer with a pH of 7 as a supporting electrolyte, which allowed for observing an enzymatic saturation extended up to 50 mM. The phosphate buffer was dripped onto the electrode and dried under a vacuum, demonstrating that such an inhibition mechanism was related to a pH variation, rather than to a substrate inhibition. Special attention has been given to sweat pH because lactate constitutes on average 0.28% of sweat and contributes to its acidity.

Wang et al. [68] proposed a wearable biosensor based on lactate sensing for skin Bluetooth real-time monitoring of perspiration in vivo. They evaluated the effects of pH variations of sweat on the sensing device. To solve this problem, they covered the electrode surface with extensive and uniform Prussian blue and reduced the graphene oxide membrane, which increased the sensor stability. They evaluated the long-term stability of the biosensor by measuring the sensitivity every four days over 20 days and the sensitivity remained 88.3% of the initial value after multiple uses in 20 days. Additionally, the membrane was formed by urchin-like Au nanoparticles and lactate oxidase (LOx). The urchin-like Au particles improved electron transport from the enzyme active centre to the electrode.

To improve the sensor operational response time, especially for continuous monitoring biosensors, Hojaiji et al. [72] presented a compact multicompartment wearable system to study diurnal variations in sweat glucose levels in relation to daily food intake. The enhancement of this work was the use of the multicompartment, in which each compartment could be activated to autonomously induce or modulate sweat secretion via iontophoretic actuation and analyse sweat at set time points. This ability allowed for improvement of the sensor operational response time. This system was developed following a hybrid-flex design and a vertical integration scheme, integrating the required functional modules: miniaturized iontophoresis interfaces, an adhesive thin film microfluidic-sensing module, and control/readout electronics. Each compartment could be programmatically activated at intermittent time points to obtain biomarker data.

Motosuke et al. [6] developed a microfluidic lactate sensing system for the continuous monitoring of sweat lactate. The screen-printed sensor, based on graft-polymerized MgO-templated mesoporous carbon (GMgOC), had the enzyme lactate oxidase and the redox mediator 1,2-naphthoquinone immobilized. The large surface area of mesoporous carbon and the easy covalent binding of the enzyme translated into high response currents.

To improve the stability of the sensor the authors added sucrose, catalase and PEGDGE. The sucrose stabilized the enzyme structure, thus extending the storage stability; catalase increased the operational stability of oxidase-based sensors by deactivating the hydrogen peroxide produced by the oxidase when oxygen was used as the electron acceptor; and the cross-linker PEGDGE enhanced the immobilization efficiency of LOx and catalase. They also emphasized the use of PDMS as a substrate for the sensor because this material is soft and comfortable to wear for extended periods of time (6 h) without causing skin irritation. Furthermore, the PDMS prevented sensor chip bending when the sensing system was attached to slightly curved body parts, such as the upper torso (front or back) or upper limbs (arms or legs).

Qi et al. [4] developed smart glasses with an enzymatic biosensor for low-noise and non-invasive determination of lactate in human sweat during physical exercise. A bi-enzyme gel membrane was casted on a polypropylene (PP) substrate and was attached to the arm of a pair of eyeglasses. Lactate was measured during cycling exercise for 30 min by connecting the three-electrode biosensor with an electrochemical analyser.

4.3. Selectivity: Chemical Interferences

Sweat is a complex medium that consists of metabolites and electrolytes, and it usually contains only traces of electroactive substances, such as ascorbic acid, acetaminophen, and uric acid, which may disturb the electrochemical determination of analytes and lead to inaccurate current readings [24,69]. Reports on sweat sensors have investigated the effects of interfering electroactive substances only in the micromolar range. Thus, it is reasonable to expect that negligible interference will distort the sensor signal during field testing on healthy people. However, these electroactive substances can interfere with the sensor signal when monitoring athletes during exercises or in unhealthy people.

Qi et al. [24] analysed common electroactive physiological interferents, such as ascorbic acid, glucose, and uric acid in lactate sweat sensors. They found an insignificant current interference, indicating excellent discriminatory selectivity of the biosensor.

Ye et al. [33] developed a wearable electrochemical sensor for real-time monitoring of sweat glucose, using a three dimensional paper-based microfluidic electrochemical integrated device. They analysed the presence of interferences, such as 0.1 mM NaCl, 2 mM uric acid, 2 mM ascorbic acid, and 5 mM lactate. The sensor did not present any significant interference signals in the glucose signal, and they attributed this result to the modification of the electrode surface. The working electrode was modified with Nafion; and then a chitosan layer, the enzyme glucose oxidase, and the mediator Prussian blue were immobilized on the modified electrode; and finally a layer of chitosan was casted. They argued that the Nafion layer was critical to remove interferences present in sweat. Molecules with a molecular weight higher than that of H_2O_2 , such as ascorbic acid and uric acid, could not penetrate the lattice and follow a redox reaction.

5. Sensing Biomolecules in Sweat with Affinity Electrochemical Biosensors

Immunosensors are biosensors that incorporate antibodies as biorecognition elements [66]. They have been used to detect the presence of intermediate-size organic molecules and biomolecules, such as steroid hormones, drugs of abuse and their metabolites [86], and macromolecules (proteins, interleukins, enzymes) [87]. The most usual electrochemical transduction technique is either voltammetry or electrochemical impedance spectroscopy. The main compounds present in sweat, which are being studied to be detected with wearable immunosensors, are cortisol, cytokines, ethyl glucuronide, and drugs of abuse [87]. Amongst these different analytes, a great amount of work has been especially performed to determine cortisol. Cortisol is a steroid hormone playing a key role in homeostasis, and it has been related to stress-based diseases and disorders. On the other hand, cytokines are a broad group of small proteins that play important roles in cell signalling, modulating immune responses. Consequently, cytokine sweat sensors have been developed for the diagnosis of diverse inflammatory processes. Finally, sweat immunosensors have been also developed for the detection of ethyl glucuronide (a metabolite of ethanol) and drugs of abuse (such as methadone, methamphetamine, amphetamine, and tetrahydrocannabinol).

Different approaches have been used in sweat analysis based on affinity biosensors, most of them employing antibodies as biorecognition elements, although aptamers have also been used. Figure 7 schematically shows two of the main strategies used for the label-free detection of a given analyte acting as an antigen. One usual strategy is to detect the formation of antibody-antigen complexes with the aid of a reversible redox probe (Figure 7a). The electrode surface onto which antibodies are immobilized is accessible to the redox probes, and they can conduct electron transfer reactions at the electrode. These processes can be followed by diverse electrochemical techniques, such as chronoamperometry, CV, DPV, and EIS. The formation of antigen-antibody complexes blocks the access of the redox probes to the electrode surface, and consequently the current decreases in amperometric or voltammetric signals (i.e., the electron transfer resistance increases).

Immunosensors often include the use of nanomaterials, which provide a larger electroactive area, to improve sensitivity and the limits of detection. Santiago et al. [88] developed an immunosensor based on graphene oxide, which was further modified by covalent linking of protein A, which in turn was employed to immobilize cortisol antibodies. $K_4Fe(CN)_6$ was used as a redox probe, and the decrease in the anodic and cathodic peak in a cyclic voltammogram was sensitive to cortisol in the 0.1–150 ng/mL range. Laochai et al. [89] developed an immunosensor based on L-cys/AuNPs/MXene conductive thread electrodes with covalently immobilized cortisol antibodies. An enhanced area was achieved with MXene and AuNPs, and chronoamperometry was used to determine cortisol levels, employing $Fe(CN)_6^{3-/4-}$ as a redox probe, obtaining a linear range of 5–180 ng/mL and an LOD of 0.54 ng/mL. Madhu et al. [90] developed a cortisol biosensor based on carbon yarns coated with zinc oxide nanorods, presenting high mechanical stability and superwettability. After cortisol antibodies immobilization, cortisol levels were determined using CV and DPV, again with $Fe(CN)_6^{3-/4-}$ as a redox probe, obtaining a linear range

from 1 fg/mL to 1 $\mu\text{g/mL}$ and an LOD of 0.45 fg/mL by CV and 0.098 fg/mL by DPV. Additionally, Madhu et al. [91] employed a similar approach with TiO_2 nanostructures combined with carbon yarns, obtaining a linear range from 10 fg/mL to 1 $\mu\text{g/mL}$.

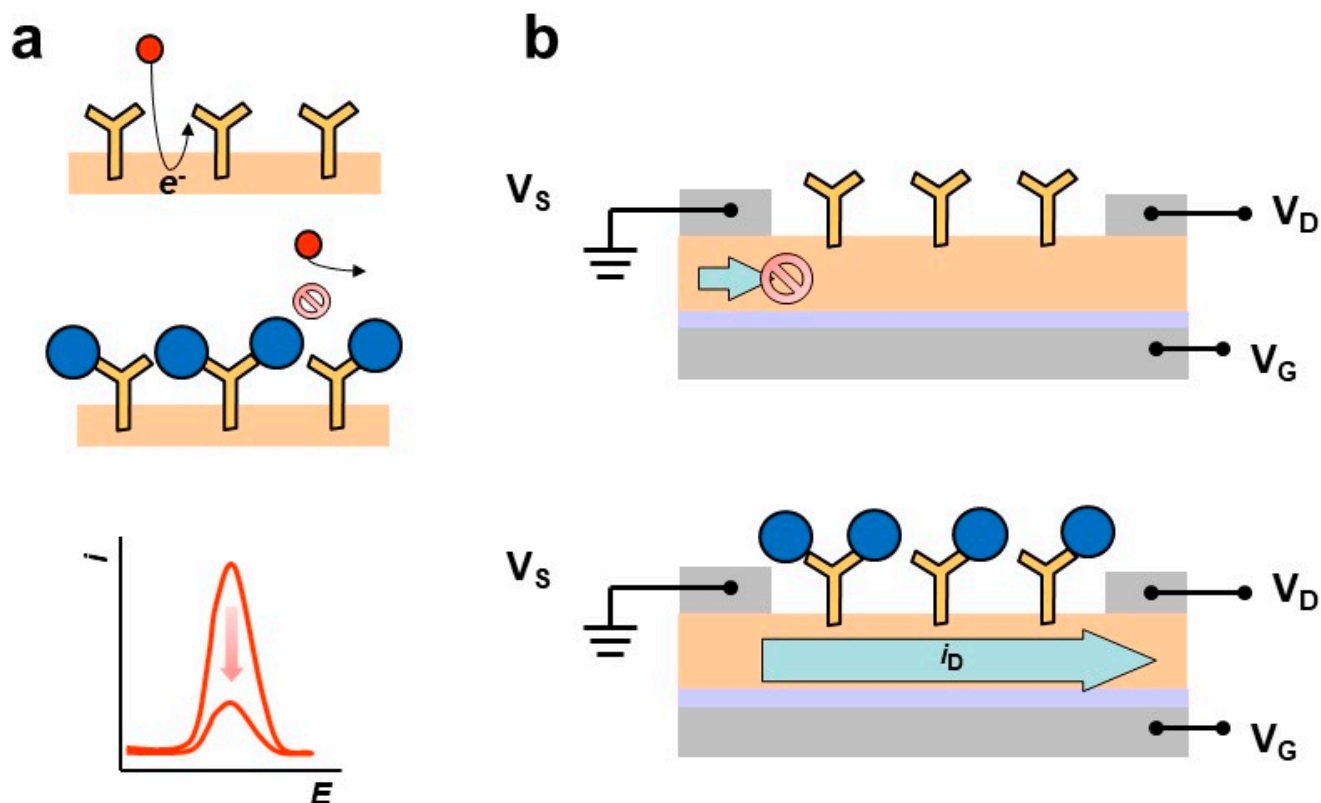


Figure 7. Schematic representation of two label-free immunosensors designs employed in sweat biosensors. (a) The formation of antibody-antigen (in yellow and blue, respectively) complexes can be detected indirectly since they block the electrode surface to the passage of a redox probe (red) and diminish current signals due to electron transfer reactions, a process that can be followed by voltammetric or impedimetric techniques (e.g., SWV, as shown in the figure). (b) Field-effect transistors allow for direct detection of the formation of antibody-antigen complexes (for instance, by measuring the drain current under appropriate conditions).

Microfluidic channels have been included in several sweat sensors to improve sample collection. Naik et al. [92] presented a microfluidic platform for cortisol detection and continuous glucose monitoring. Adhesive microchannels and an inkjet-printed graphene sensing electrode, with the possibility of incorporating electrowetting valves, were integrated with a synthetic skin to produce a “smart bandage”. Au nanoparticles were deposited onto the surface of graphene electrodes and cortisol antibodies were covalently immobilized. The cortisol levels were determined by chronoamperometry for a $\text{Fe}(\text{CN})_6^{3-/4-}$ redox probe, and an LOD of 10 pM was achieved for cortisol in sweat. Nah et al. [93] developed a wearable immunosensor that included a microfluidic channel and chamber. $\text{Ti}_3\text{C}_2\text{Tx}$ MXene-loaded laser-burned graphene flakes were transferred onto a PDMS substrate, and cortisol antibodies were covalently immobilized. Cortisol concentrations in artificial sweat were determined by EIS, obtaining a linear range of 0.01–100 nM and an LOD of 88 pM.

Cheng et al. [94] developed an immunosensor based on flexible screen-printed electrodes, onto which AuNPs were electrochemically deposited, and cortisol antibodies were covalently immobilized via a HOOC-PEG-SH linker. Cortisol levels were detected by DPV, employing $\text{Fe}(\text{CN})_6^{3-/4-}$ as a redox probe, and an LOD of 7.47 nM was obtained. However, the emphasis of the work was on the construction of a complete wearable cortisol sensor, including aspects not usually covered in publications on electrochemical sweat sensors,

such as the need for a portable, miniaturized, low consuming electronic instrumentation capable of processing the transduced signal and communicating the results to the user (Figure 8).

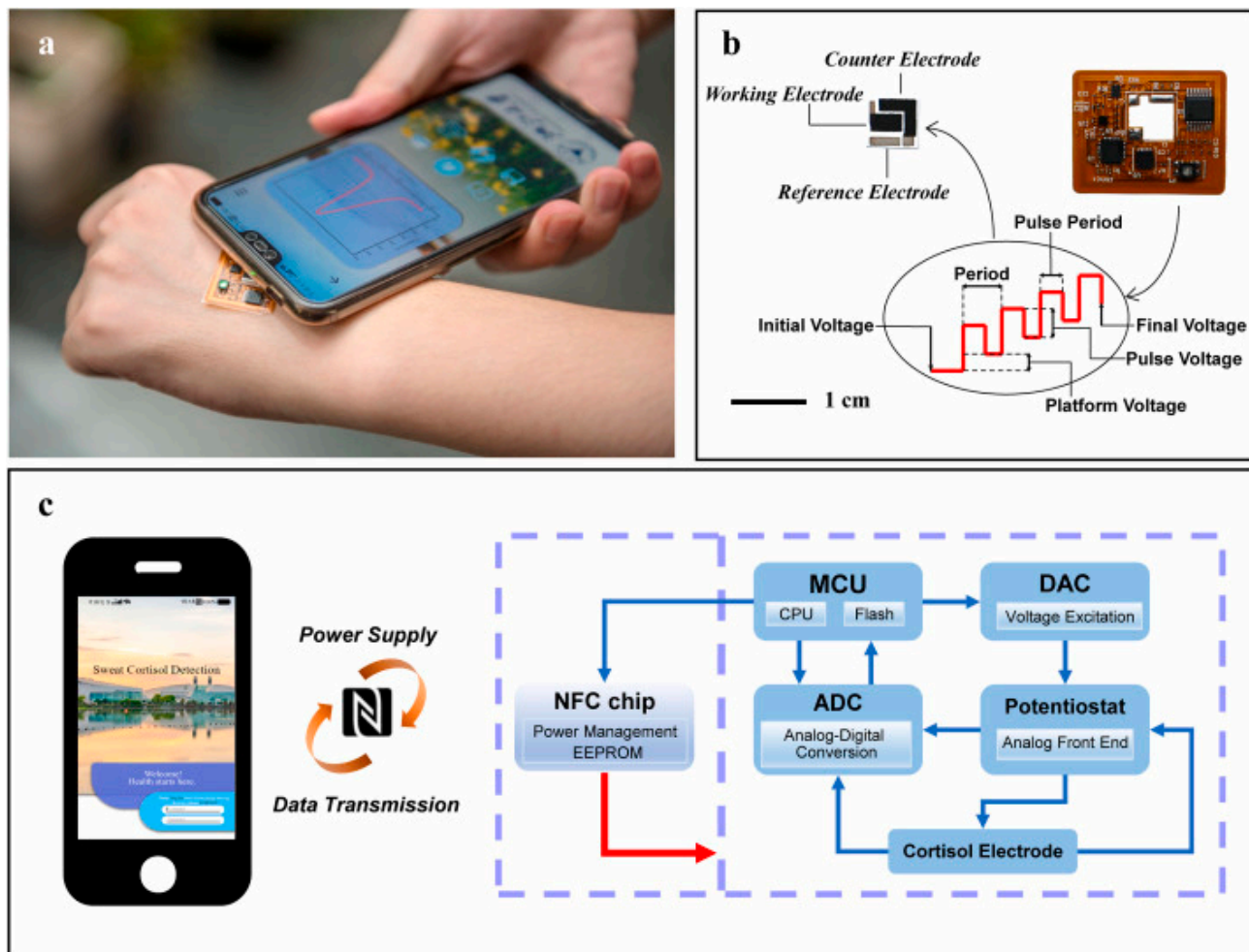


Figure 8. The integrated wireless, battery-free, and flexible detection system with NFC-enabled smartphone. (a) An image of in situ detection of sweat cortisol; (b) the flexible sensing system for electrochemical detection of cortisol; (c) block diagram of the wireless, battery-free, and flexible patch. Reprinted from Ref. [94]. Copyright (2017), with permission from Elsevier.

Cortisol aptamers have also been used as biorecognition elements. Ganguly et al. [95] developed an impedimetric aptasensor for the determination of sub-microlitre passively eluted sweat. Aptamers were bound to a ZnO-modified electrode, and cortisol levels were determined by EIS. A dynamic range of 1–256 ng/mL was obtained.

Another strategy is based on the use of field-effect transistors (FETs). This approach has additional advantages compared to those systems employing an auxiliary redox probe, such as direct detection of the formation of antigen-antibody complexes (Figure 7b). The use of transistors is especially attractive in biosensors because of the possibility of miniaturization and achieving high sensitivity and extremely low LODs when used in combination with nanomaterials. Demuru et al. [96] developed an immunosensor based on a cortisol antibody modified organic transistor, obtaining sensitivity of 50 $\mu\text{A}/\text{dec}$ (Figure 9).

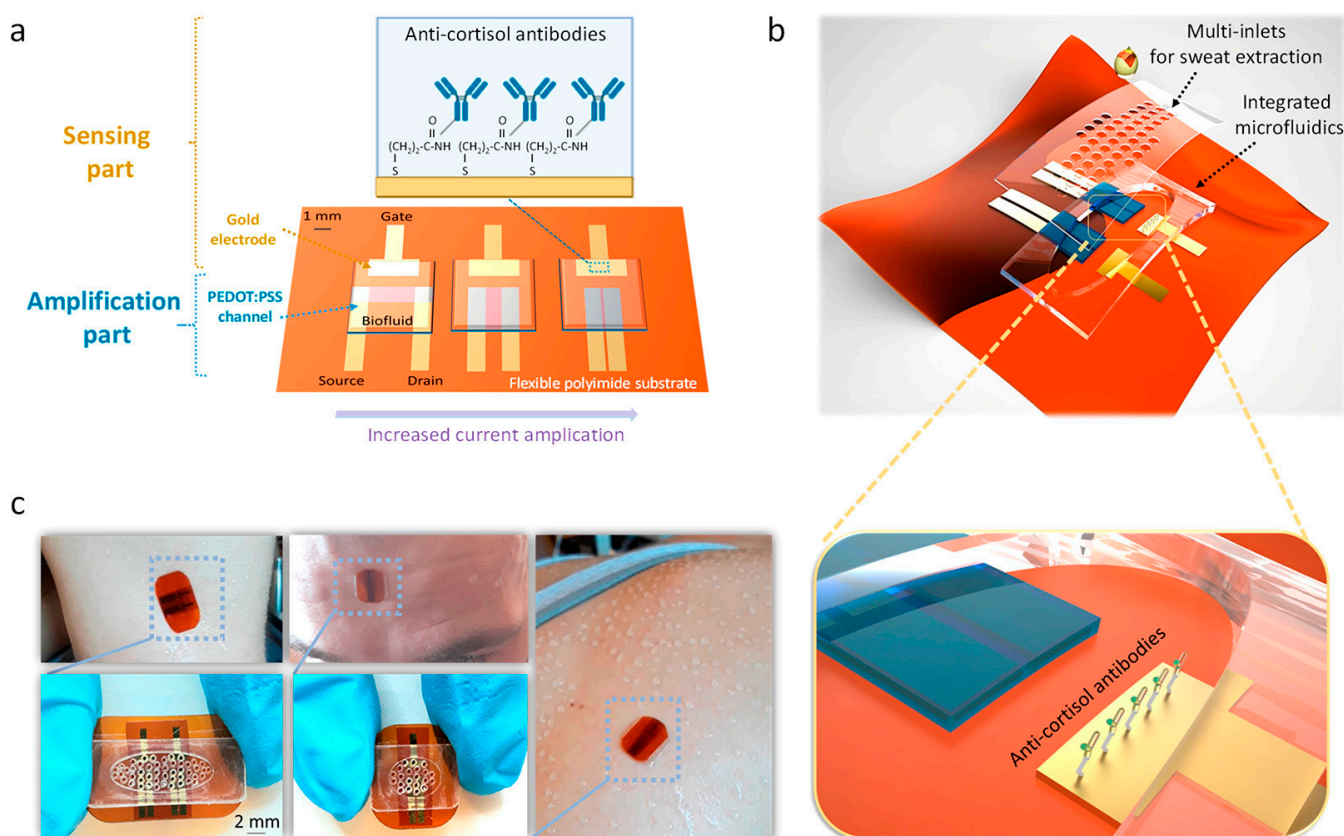


Figure 9. Organic transistor structure and sticker application. (a) Schematic of the biosensing principle involved and structure of the OECT devices, including antibody-coated gate electrodes and the organic PEDOT:PSS channel for current amplification; the latter shows three OECT devices with different PEDOT:PSS channels of an increased width per length ratio. (b) 3D-image with two OECTs integrated into a microfluidic system for direct sweat collection and zoom of the gate electrode with the anticortisol antibody immobilized. (c) Application of a cortisol sensing sticker on the human skin for sweat collection during sports activities; the microfluidic part with the multiple inlets is placed in contact with the skin. Reprinted with permission Ref. [96]. Copyright (2022), American Chemical Society.

In the next section, we address issues such as electronic signal processing, wireless communication, and power supply in connection to electrochemical sweat sensors.

6. Electronic Instrumentation

Once the sample extraction, collection, transport, and detection stages have been established, signal processing and transmission need to be performed. For portable, non-invasive, rapid, and real-time monitoring applications in the field, the use of heavy, bulky, and non-portable laboratory equipment for signal processing is not suitable. For this reason, there is great interest in researching and developing thin and light embedded wearable sensors with advanced electronic technologies that incorporate miniaturized circuitry, wireless transmission systems, and more efficient power modules [7,19,97–101].

6.1. Integrated Electronics

Electronic instrumentation processes the electric signals produced after the transduction of chemical or physical signals (physiological, biochemical, environmental, etc.). These electrical signals are conditioned by going through different amplifiers and filters to reduce spurious signals and noise. This process is responsible for signal processing and data logging management using microcontrollers (μC), memory systems, and analogue-to-digital and digital-to-analogue converters (ADC/DAC) that work together to adapt and control

the flow of signals. In addition, they must handle the communication with different devices and the data transmission for subsequent analysis and visualization [102,103]. The main components of a wearable sensor and their interaction can be represented schematically in a block diagram, as shown in Figure 10. Colburn et al. [104] explained, in a detailed introduction, how they work and the most important characteristics of these components to correctly understand the electrical signals resulting from experimental measurements.

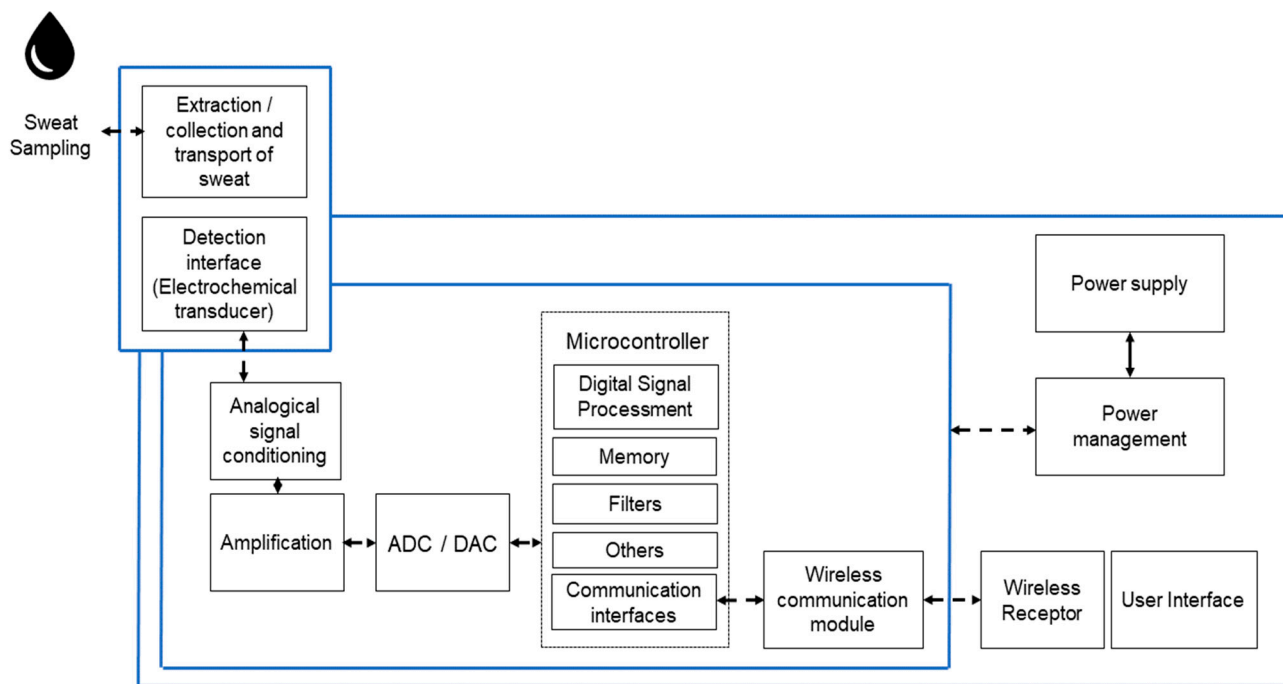


Figure 10. Fundamental blocks of a wearable electrochemical sweat sensor.

To characterize (bio)sensors, typically using amperometric and voltammetric techniques, the use of a potentiostat is required, which can be described as an instrument that permits control of the working electrode potential with respect to a reference electrode, by applying a potential difference between the working electrode and an auxiliary electrode. Additionally, the current flowing through the working electrode must be measured.

Focusing on such scenarios that require this type of portable device, a wide variety of potentiostats have been developed, prioritizing in each case the most relevant characteristics, depending on the application or the use for which they were created. Some of them stand out for their measurement ranges and others for their precision, level of integration, portability, ease of use, configuration possibilities, accessibility, cost, and so on.

There are portable potentiostats on the market capable of conducting most electrochemical techniques [105–107]. However, this type of equipment is not accessible for the widespread use in research or education settings (>US \$1000). For these cases, cheaper devices are required, which have limitations (resolution, ranges, etc.) but allow for the most used electrochemical characterizations to be performed. There is even a trend in open-source portable devices of this type, which makes the knowledge generated available to the entire community. The main characteristics of some of them are shown in Table 5 [108–112].

The first potentiostats developed were based on analogue circuits with different discrete components, which were configured as simple blocks that interact with each other without any type of programming complexity, requiring additional hardware to obtain, send, and display the signals. Later, potentiostats that based their processing logic on microcontrollers began to be developed, also incorporating amplifiers and ADC and DAC converters to digitize and condition the signals to subsequently interact with digital communication protocols. The whole system was mounted on a printed circuit board

(PCB) or another kind of substrate, thus forming a final device capable of performing electrochemical measurements [108,111–113].

Table 5. Characteristics of open-source potentiostats.

Name	Power	Communication	User Interface	Range	Resolution	Ref.
UWED	Lithium polymer rechargeable battery (LiPo)	Wireless with protocol “Bluetooth Low Energy” (BLE)	Smart phone/tablet	± 1.5 V, ± 180 μ A	67 μ V (40 μ V noise); 6.4 nA (30 nA noise + nonlinearity)	[109]
DStat	USB	Wired connection via USB/serial port	PC—multiplatform software	± 1.5 V; lowest limit of detection 600 fA (7 ranges)	46 μ V; \sim pA	[111]
CheapStat	USB	Wired connection via USB/serial port	PC and three-line display + joystick	2990 mV a 990 mV ($\sim \pm 1$ V); ± 100 nA and ± 10 μ A (2 ranges); 1 to 1000 Hz	\sim mV; \sim nA	[112]
USB-controlled potentiostat/galvanostat	USB	Wired connection via USB/Serial port	PC—multiplatform software	± 8 V, ± 20 mA, ± 200 μ A and ± 2 μ A; sample rate: 90 ms	(DAC: 20 bits/ADC: 22 bits) 15.3 μ V; 12 nA, 120 pA and 1.2 pA and noise: 88 nA, 1.1 nA and 9.9 pA	[110]
MYSTAT	External 15 volt DC	Wired connection via USB/serial port	PC—multiplatform software	± 12 V; ± 200 mA	-	[108]

Jenkins et al. proposed a topology in which an AD5933 was used to measure the impedance of the electrochemical cell, in addition to working as a signal generator, while some authors [29,114–116], looking for a higher level of integration, decided to use an analogue front end (AFE) integrated on a chip as a potentiostat, e.g., LMP91000/LMP91002 from Texas Instruments [117]. These devices allowed for working in a current range between ± 5 μ A and ± 750 μ A, operating in a voltage range of 2.7 V to 5.25 V, and being able to apply a bias programming voltage in the range of 0 to 24% of its reference voltage (VREF) or VDD, in steps of 2%. Therefore, considering a VREF of 3.3 V (a very common supply voltage value), the voltage sweep would be ± 792 mV with steps of 66 mV. If higher resolution is required, an external DAC with a higher bit count must be added. Physically, it comes in a 4×4 mm WSON package with 14 connection pins, pad dimensions of 250×600 μ m, and a 500- μ m pitch. Finally, with a higher level of integration and design specificity, there are potentiostats based on application specific integrated circuits (ASICs) [118,119], such as ADuCM355 from Analog Devices [120], in which the AFE and all of the digital processing blocks were integrated into a single chip. This design has the advantage of reducing the noise produced by the electrical connections between the components and a size reduction of the entire system in general, presenting a package of 6×5 mm, a 72-lead LGA, and 250- μ m and 500- μ m pitch. This model also allows for achieving an ultra-low consumption configuration, while maintaining high processing performance. It can be noted that this kind of ASICs can achieve measurement currents from ± 0.00005 μ A to ± 3000 μ A and apply voltages of ± 2.2 V with a 12-bit resolution (<1 mV).

In cases in which EIS is the transduction technique, as a complement of the microcontroller, a high-precision impedance converter system is used, such as the AD5933 (Analog Devices) [121], which generates the voltage sweep signals (27-bit DDS: Direct Digital Synthesis) with frequencies from 1 kHz to 100 kHz. On the other hand, if it is required to work with lower frequencies, it is necessary to add an external clock [122,123].

In wearable-type applications, the electronics should go along with the sensing system, generating a comfortable user experience with good mechanical performance, light weight, easiness to adapt to the body, and an extended shelf life, using suitable materials to ensure

biocompatibility. These types of devices are those that Ling et al. called “next-generation wearables” or “wearables 2.0” [99].

Before achieving the characteristics proposed by Ling, we can mention the works of Gao et al. and Vinoth et al. as part of the state of the art of multi-parameter wearable devices [7,124]. To attain this multiplicity of information without exceeding the number of components and physical volume, Vinoth et al. benefitted from the use of a μC (CC2640, from Texas Instruments), which integrates a signal processing module and a BLE (Bluetooth Low Energy) communication module. It also uses a strategy combining DAC and Op-amp configured in a way that allows for amperometric measurements (e.g., for the amperometric determination of glucose and lactate concentrations), together with the differential amplifiers used as micro-voltmeters to measure pH signals and Na^+ and K^+ sensors. Gao used a similar strategy, adding a resistor that also measures body temperature by voltage difference.

6.2. Power Supply

It is critical to have proper power control in portable devices since they must operate continuously without being connected to a power supply and, in many cases, for long periods of time. As we increase the number of functionalities, the detection of multiple parameters at the same time, a complex data analysis, sampling rates, different communication protocols, and data transmission, power management becomes a critical issue [125,126].

Krorakai et al. [127] used an alternative approach to create a near-field potentiostat in a credit card-like design ($5.5\text{ cm} \times 8.6\text{ cm}$). Based on a SiC4341 NFC chip (Silicon Craft Technology PLC) and using a connector for the electrodes and an NFC antenna for connection with smart devices (phones, tablets, etc.), this device is an example of a passive device that operates without batteries that remarkably minimizes and optimizes interconnections. In this case, the passive device is powered from the wireless NFC connection from the smart device, and it is operated remotely from a user-friendly Android mobile application. The application allows for establishing the conditions for the electrochemical characterizations to be conducted in the device within a limited range of current ($\pm 20\ \mu\text{A}$) and voltage ($\pm 0.8\text{ V}$) generated from the DAC, which has a full-scale voltage value of 1.28 V with steps of 5 mV . A similar approach was used by Bandodkar et al., although it attained a lower level of integration. In a 32-mm diameter area and with an approximate weight of 1 g , they developed a skin-interfaced microfluidic/electronic system with a microcontroller (F430FRL152H from Texas Instruments) and other discrete components, which were powered through a coil fabricated in a flexible printed circuit board (FPCB) by NFC technology [128].

With respect to the power source, rigid lithium-ion batteries (Li-ion) are most commonly used in portable devices, with a proper performance and shelf life and fast charge and discharge cycles. On the other hand, these kinds of batteries are not as adaptable to flexible wearables devices, which require quite demanding physical and mechanical operating conditions, such as bending, twisting, folding, and stretching. It must be taken into account that, normally by reducing the physical size of the device, the necessary storage energy is also reduced; therefore, it is possible to use other alternatives to batteries. A typical example for disposable, non-rechargeable use is the CR2032 lithium-ion coin-cell battery (commonly used in watches and portable devices), which has a charge of 225 mAh and an operating voltage of 3 V , and it is widely used due to its small size (approx. 20 mm in diameter, 3.1 mm in thickness and a weight of 2.9 g) and low cost.

The rapid development and evolution of wearable sensor technology, which has spread to many applications in recent years, have required a huge effort in terms of research and development of rechargeable and flexible batteries, seeking to improve power density, charge cycling, and energy efficiency, as well as achieving a greater degree of flexibility to obtain a more adaptable and comfortable device. New materials (flexible, stretchable, more efficient, and environmentally friendly) and processing techniques were tested and implemented [129,130]. On the other hand, flexible substrates, such as elastomers, textiles,

and paper, have been studied, as well as their application in new energy accumulators (batteries, supercapacitors, etc.) and energy harvesting (solar cells, biofuel cells, movement systems, etc.) [126,131–134]. The review of Kong et al. [135] summarizes the most recent advances in terms of flexible batteries, giving a complete characterization regarding their mechanical properties and how they affect electrochemical performance, describing at a constructive level some of the most significant achievements in their critical components (electrolytes, current collectors, etc.). It also presents some cases of functional prototypes, highlighting design considerations to achieve their implementation at the industrial level. Gai et al. [131] and Song et al. [132] proposed an energy harvesting system that used the energy coming from the motion of the human body during exercise by means of so-called nanogenerators, offering powers of a some milliwatts, quite enough to process and wirelessly transmit the sensing data continuously or increase the charge of an energy accumulator (supercapacitors or batteries). Gai et al. reported that power generation systems can obtain about 60 V and 15 mA from movements at frequencies as low as 5 Hz.

It is important to emphasize that, in all these cases, a critical condition is that the energy produced by the generator must be higher than the consumption of the entire system. For this purpose, it is very important to select ultra-low consumption components and optimize both the design of the circuits and the criteria used in signal sampling and communication methods.

As we mentioned before, a substantial drawback in wearable applications is that, by reducing the size of the devices, they are limited in energy harvesting, have short lifetimes, and variations in energy efficiency. Something similar happens with biofuel cells. Supercapacitors are becoming an increasingly strong alternative for portable energy storage since they have the ability to store more energy per unit volume than batteries and have high charge/discharge cycles (>100,000), low discharge rates, low electrical resistance, higher performance, and good resistance to mechanical stress [133]. Studies in chemistry, physics, and materials science have allowed for progress with greater possibilities of fabricating robust supercapacitors with better and more appropriate materials (electrolytes, electrodes, binders, and additives), as well as packages and electrical characteristics (charge time, lifetime, leakage current, degradation, etc.). Some nanomaterials based on carbon or graphene, due to their greater surface area, good electrical conductivity, and chemical inertness, are of great interest for this type of application. Other complementary proposals that have been tested for self-powered sensors and actuators are some portable devices based on origami techniques [136]. Nevertheless, one of the great challenges that remain in this type of technology is the reduction in size and biocompatibility.

6.3. Wireless Communication

Another function that the electronic instrumentation of the device must provide is communication with the user to clearly and precisely transmit the information obtained from the sensors. In the case of the first portable devices, this transmission was usually accomplished through a wired connection using USB ports or analogue audio interface [110,111,137]. With the advance of technology and the growth of smartphones and internet of things (IoT) applications, wireless connectivity began to be used instead, as wired connections made the usability of portable and wearable devices more complicated [109]. For this type of communication, a large number of wireless protocols that respond to current IoT demands are available: Bluetooth Low Energy (BLE) [138–140], ZigBee [141], radio frequency (RFID) and near field communication (NFC) [35,142–144], Wi-Fi [145,146], and narrowband internet of things (NB-IoT) [147], of which BLE and NFC are perhaps the most widely used in wearables. However, these protocols could have limitations to being used in more complex applications that require higher information density and energy consumption. We can see in Figure 11 a comparison graph showing the relationship between speed and the range of data transmission for different communication protocols.

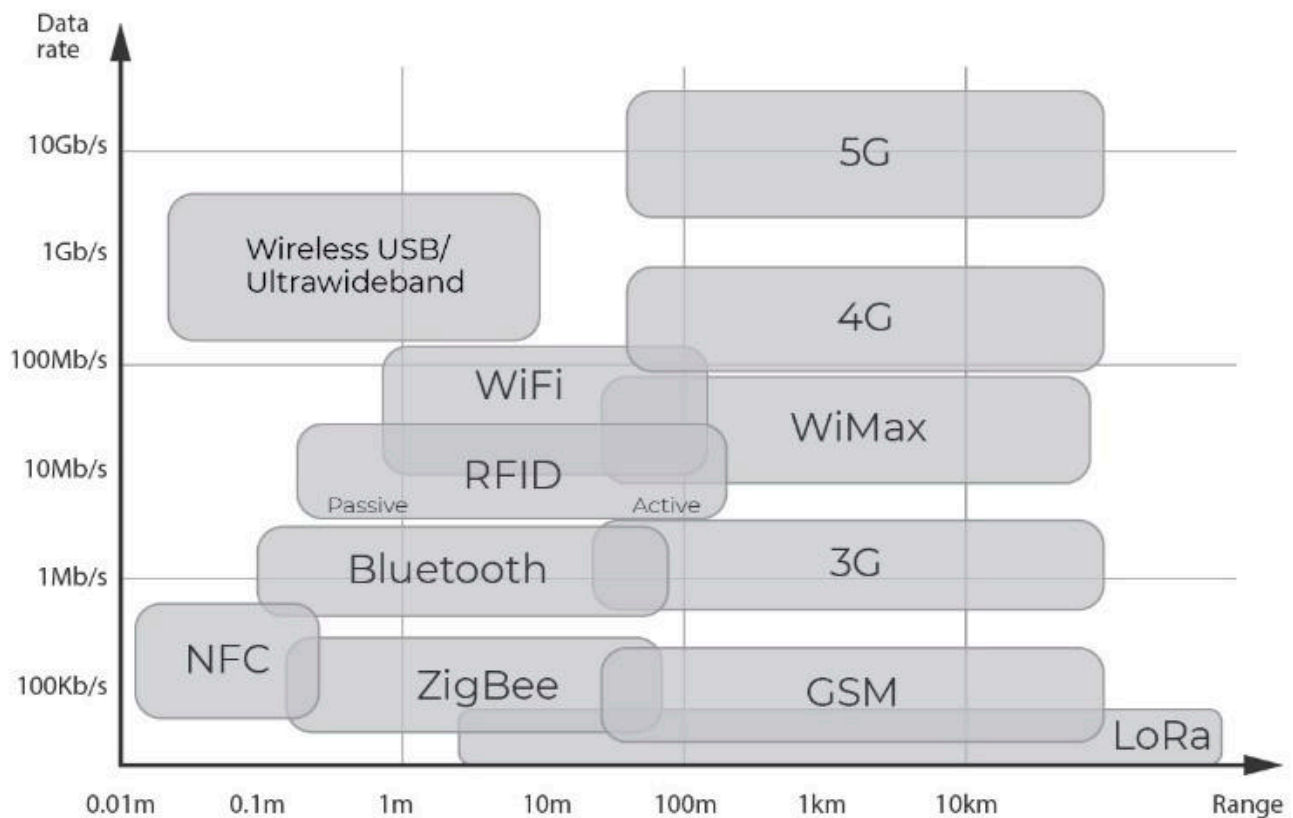


Figure 11. Data rate vs. range of data transmission for different communication protocols.

In the case of NFC communication, for example, it works at a frequency of 13.56 MHz with a data rate of 106 kbps to 424 kbps. Regarding the transmission distance, the devices should be quite close to communicate with each other since the wireless range is 20 cm or less. This technology can work in two different modes: passive mode, in which the reading device initiates the communication, and the other NFC device (tag) uses the energy of the electromagnetic field to energize itself and then exchange information; and the active mode, in which both devices have their own power sources for data communication. The advantage in the case of active mode is that, in addition, the distances between the reader and the tag can be longer. This kind of wireless communication is used in devices with simpler electronics that only need to transfer a little information to other NFC compatible devices (readers, smartphones, etc.) and do not require extra power. Among the most popular uses of this technology are smart labels, access control devices, contactless payment systems, ID documents, and smart signage. However, due to its simplicity, it is also widely used in medical applications for health monitoring, to record and monitor different vital parameters of patients autonomously. In this case, the proximity required by NFC technology makes it possible to guarantee the correct reading of data, thus reducing the chances of error or information theft. Sweat sensors are also an example of devices that have incorporated NFC technology, taking advantage of the stable operation and small size of devices with low weight and packaging options that allow for good mechanical compatibility [148,149].

In terms of improving the efficiency of this type of communication, different strategies can be used to optimize its operation from the electronic control unit, such as reducing sampling times based on the application requirements or turning off communication while the device is inactive or even combining different communication technologies (RFID, ZigBee, Wi-Fi, Bluetooth, etc.), taking advantage of each of them [126,150,151].

Regarding Bluetooth, it is a short-range, high-data rate, low-power wireless communication technology commonly found in most portable devices, such as smartphones, smartwatches, and computers. It works in the ultra-high frequency band of 2.4 to 2.485 GHz and

supports a maximum data rate of 2 Mbps [139]. In particular, the Bluetooth Low Energy (BLE) protocol was designed specifically for short communications between devices for IoT applications and devices with very limited power consumption [7,130]. BLE consumes less than 15 mA, has a data rate from 125 kbps to 1 Mbps (BLE 4.0) [152], and supports a maximum distance of 100 m from the device to the receiving station. Typical applications of this technology are personal healthcare, fitness training, entertainment, etc.

On the other hand, the technologies with the lowest energy consumption are NFC, Bluetooth, ZigBee, and Lora, and despite having a low data transmission rate, they are generally suitable for the instrumentation of this type of sensor. Finally, we can therefore say that the choice of the most convenient communication protocol for each application will depend on technological availability, costs, frequency bands, data rates, coverage, and energy consumption [99].

7. Machine Learning Signal Processing of Electrochemical Sweat Sensors

Signal processing is a fundamental tool for enhancing the performance of electrochemical sweat sensors. It consists of various steps that involve noise filtering, identification and characterization of relevant signal events, and interpretation of these signals (Figure 12). This tool, along with other strategies (i.e., the use of nanomaterials), allows for the enhancement of figures of merit of the sensors, such as LOD, sensitivity, and selectivity. However, signal processing plays a key role for establishing correct relationships between a primary signal (current, potential) and analyte concentrations, a health condition, or even prediction of a possible future event. This goal can be achieved using traditional algorithms (filters for noise reduction or deconvolution, calibration etc.), machine learning (ML) algorithms, or a combination of both. The difference between traditional and ML algorithms is that the former is based on known parameters and models and gives the same output for a given dataset from the first run, whereas the latter is based on unknown parameters that are acquired and refined through a training process.

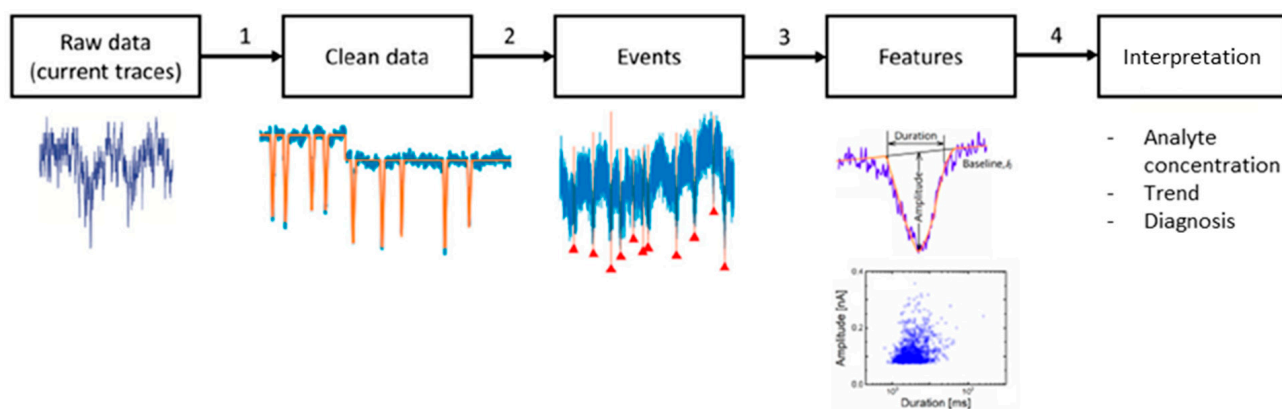


Figure 12. Four steps for signal processing: (1) noise filtering; (2) signal identification; (3) signal characterization; (4) signal interpretation. Adapted with permission from Ref. [153], Copyright 2019.

ML algorithms are limited by computational capabilities and data availability for training, but they are able to adapt to a particular sensing system and predict relationships not previously defined by a given model. Since the internet of things and cloud computing are currently solving the limitations of ML, these algorithms are gaining ground in many sensing applications and demonstrating their advantages.

ML algorithms can be classified as supervised and unsupervised learning. Supervised learning relies on training data already labelled, and a predictive model is given. On the other hand, unsupervised learning algorithms can be trained using unlabelled data and no training model. Regarding models for supervised learning, they can be classification or regression models. The former is more suitable for dividing data into classes (i.e., low,

normal, or high sweat glucose levels), whereas the latter is designed for trend forecasting (i.e., prediction of abnormal glucose levels in the future).

Regarding chemical sensors for health applications, supervised learning algorithms are by far the most used because they can operate with a relatively small training dataset, the training data can be easily labelled using state-of-the-art clinical signs and symptoms, and the computational cost is relatively low. A model classification for supervised learning is shown in Figure 13.

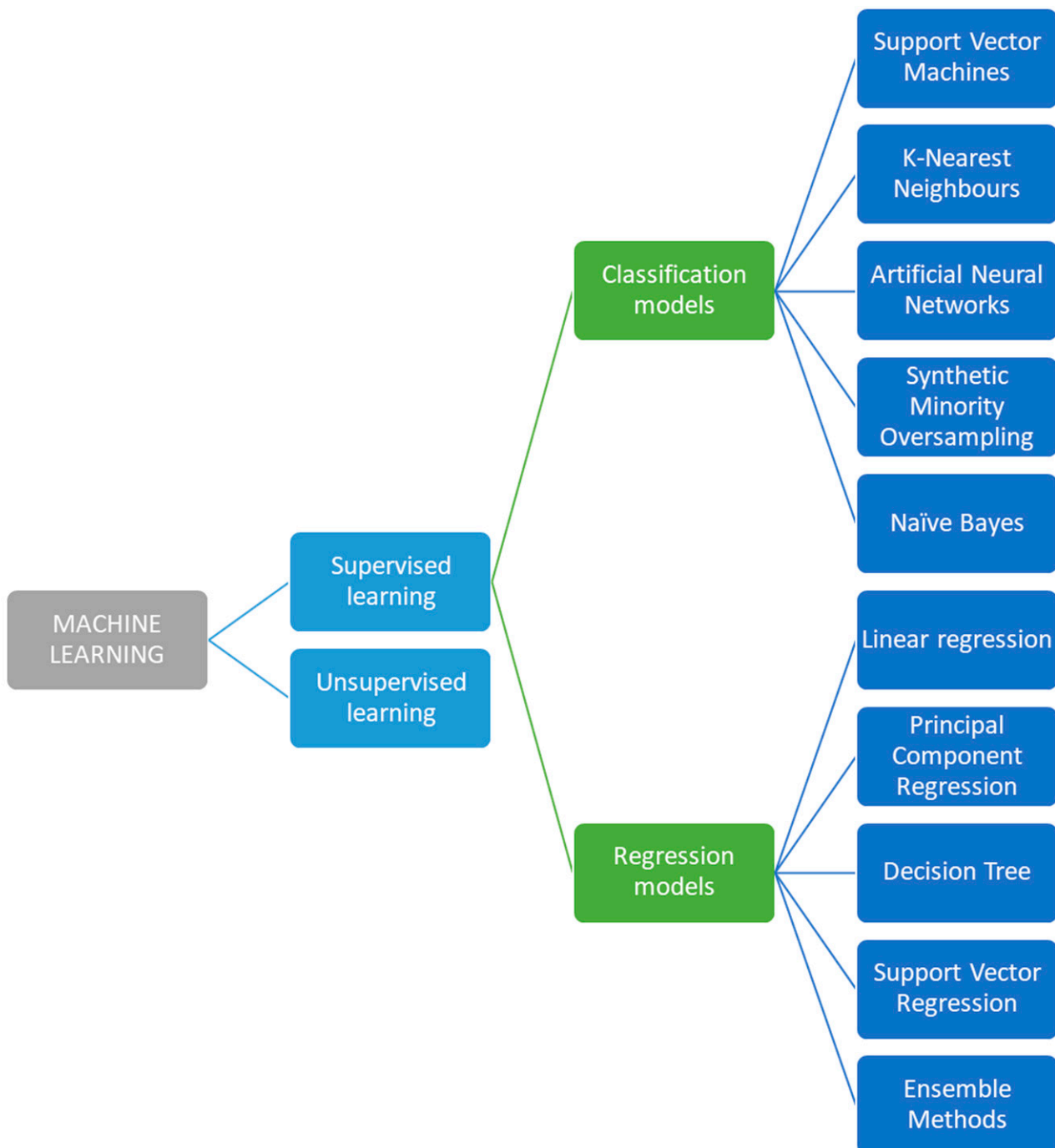


Figure 13. Classification of ML algorithms. Ensemble methods combine two or more models. Examples of ensemble methods are random forest and gradient boosting.

Electrochemical sweat sensors possess many advantages over other alternatives, such as ease of miniaturization and integration. These features allow for their implemen-

tation in wearable sensor technologies at a massive scale and continuous monitoring. Therefore, these sensors are able to collect a huge amount of data that can be processed by ML algorithms.

On the other hand, many sweat electrochemical sensors and biosensors are intended for continuous analyte monitoring due to their ability for miniaturization and integration. Electrochemical sweat sensors for continuous monitoring (ESSCMs) are able to provide a large amount of data automatically without the patient's intervention and can detect and predict health issues anytime. However, ESSCMs suffer from several limitations that condition their accuracy during their lifetimes, such as the dynamic correlation of analyte concentrations in sweat compared to other fluids that constitute a clinical gold standard, such as blood; changes in their figures of merit due to physical or chemical interferences or electrode degradation over time; and patients' personal characteristics or health condition.

From the analytical point of view, the aforementioned limitations can be circumvented by periodic external calibration. However, external calibration is a severe restriction for the application of ESSCMs because it causes discomfort to the patient and cuts down on the main advantage that ESSCMs have in terms of user experience.

The case of continuous glucose monitoring is very relevant because of the high incidence of diabetes among the global population (9.3%) [154] and the huge market for portable devices for glucose testing. For instance, the FreeStyle Libre[®] Flash Glucose Monitoring System was developed by Abbot for the continuous monitoring of glucose in interstitial fluid. This sensor did not show significant subject-dependent variations in sensitivity and mean absolute relative difference (MARD). The overall MARD compared to blood glucose reference was 11.4%. The correlation with blood glucose had a slope of 1.02, an intercept of -6.4 mg/dL, and a correlation coefficient of 0.95 within a range of 23 to 498 mg/dL. This system has a factory calibration and allows algorithmic correction for the measured analyte data during its 14 day use period [155]. Moreover, this sensor is able to predict short-term trends in glucose levels, which is very important for patients to minimize the occurrence of hyperglycaemia and hypoglycaemia. Although this sensor monitors glucose levels in interstitial fluid, it is relevant in that it performs continuous monitoring and has been developed on a commercial scale. For the case of this sensor, long-term predictions were made employing machine learning algorithms, which are very relevant for the prediction of nocturnal hypoglycaemia in diabetic patients [156]. The FreeStyle Libre[®] sensor data were combined with data from a wearable physical activity tracker.

The main problems regarding FreeStyle Libre[®] and similar sensors are that they are still invasive, and their application to preventive medicine is still limited. Regarding the former, ESSCMs can be used as a non-invasive alternative for continuous monitoring of glucose, as well as many other analytes. Regarding the latter, ML algorithms are very useful tools for establishing trends in a patient's condition and prescribing preventive treatments.

A major issue with sweat sensors is that there are many interferences that affect the measurement of analytes, such as movement, temperature, and humidity. Regarding accuracy, a multisensor approach has been proposed by many research groups [157]. The problem with using various sensors is they provide increased noise levels. For this reason, there are many noise-cancellation algorithms, such as Kalman filter, Fourier analysis, or moving average filter.

Clark error grid analysis has been extensively used as a gold standard for clinical validation of glucose meters. According to this analysis, the accuracy of glucose meters should be within 20% of the true value. Accuracy of this order of magnitude is expected for other analytes, including those present in much lower concentrations compared to glucose, such as cytokines [158].

Application of ML algorithms to electrochemical sensors as solutions for enhancing their selectivity and LOD, calibration, continuous monitoring, establishing trends, and predictions of many clinically relevant analytes from measurements of body fluids have been reported in recent literature. Some of these recent works are summarized in Table 6.

Table 6. Recent applications of ML for the optimization of monitoring relevant analytes from body fluids using electrochemical sensors. EIS: electrochemical impedance spectroscopy.

Type of Sensor	Monitored Parameters	Monitored Fluids	Calibration/Prediction Strategy	Reference
Potentiometric	Chloride, skin temperature, core temperature, heart rate	Sweat	External calibration, principal component analysis, random forest	[159]
Chemoresistive (MOS type gas sensor)	Ethanol, methanethiol, ammonia, trimethylamine	Sweat (gas phase)	Principal component analysis, synthetic minority oversampling technique, support vector machine, decision tree, K-nearest neighbours, naïve Bayes classifier	[160–162]
EIS	Glucose, skin temperature, relative humidity	Sweat	Linear regression, ensemble regression, decision tree	[163]
EIS	Cortisol, skin temperature, relative humidity	Synthetic sweat	External calibration, K-nearest neighbours	[164]
EIS, Amperometric, Chemoresistive	Glucose, pH, relative humidity	Sweat	External calibration, K-nearest neighbours	[165]
Amperometric	Creatinine, heart rate	Sweat	External calibration, algorithm not specified	[166]
Potentiometric	pH	Wound	Linear regression, K-nearest neighbours, decision tree, random forest, gradient boosting, artificial neural network	[167]
Amperometric	Tyrosine, uric acid	Sweat, saliva	Linear regression, support vector regression, Bayesian regression, K-nearest neighbours, decision tree, random forest	[168]
Amperometric	Creatinine	Tears	Linear regression, K-nearest neighbours, decision tree, random forest, gradient boosting, artificial neural network	[169]
Potentiometric	Na ⁺ , K ⁺ , Li ⁺ , Pb ²⁺	Emulated dataset	Support vector regression, artificial neural network	[170]

For instance, Choi et al. proposed a multisensor approach combined with machine learning for the prediction of dehydration during exercise. They used a potentiometric chloride sweat sensor combined with a heart rate sensor and a skin temperature sensor [159].

Sabilla et al. used a set of commercial MOS-type gas sensors to build an electronic nose for sweat analysis [160–162]. The gas phase of sweat from the armpit was sampled using a vacuum pump searching for volatile metabolites produced by bacteria present in the axilla region (ethanol, methanethiol, ammonia, trimethylamine). It should be noted that, in this case, the target analytes were not analysed individually, and the sensors had many cross-sensitivities. The aim of this work was to train this electronic nose for classification of human gender using ML algorithms. The best accuracy (96.15%) was obtained using the naïve Bayes classifier.

The use of ML algorithms allows for the monitoring of analytes in sweat by correlation with other electrochemical measurements than selective potentiometric or amperometric response. For instance, Sankhala et al. developed a sweat glucose sensing platform based on electrochemical impedance spectroscopy combined with skin temperature and relative humidity [163]. In this case, the decision tree algorithm provided better predictions of glucose levels.

Another example of the application of ML to electrochemical impedance spectroscopy was described for the monitoring of cortisol levels in sweat [164]. In this case, a label-free immunosensor containing gold nanoparticles with the immobilized cortisol antibody. Zmod was used as the only input signal, and the K-nearest neighbours algorithm was used. The sensor was calibrated and then trained and tested using synthetic sweat samples, showing accuracy for distinguishing low, medium, and high cortisol concentrations within the range 8–140 mg/mL.

Sensors based on the same material can be used for simultaneous detection of different parameters. For example, a flexible wearable sensor platform based on ruthenium sulphide nanoparticles as a sensing element was developed for the monitoring of the pH, glucose levels, and relative humidity of skin [165]. The sensor was calibrated externally and was able to quantify glucose within the range of 10 Nm–1 mM and measure the pH of sweat between 4 and 8.5. The K-nearest neighbours algorithm was used for data processing and provided simultaneous monitoring of these three parameters.

ML algorithms can be used for the prediction of stress based on sweat monitoring. For instance, Kalasin et al. [166] developed a wearable electrochemical sweat sensor for continuous monitoring of creatinine. This sensor was based on poly(3,4-ethylenedioxythiophene) polystyrene sulfonate (PEDOT:PSS) and cuprous oxide nanoparticles and was able to quantify creatinine in sweat within the range 0.4–960 μ M. Creatinine concentration was used in combination with heart rate for the prediction of heat stress.

In another ML-assisted approach for the detection of creatinine, a cotton fibre electrode system was fabricated and integrated to eyeglasses [169]. The working electrode consisted of a cotton fibre with carbon black, cuprous oxide nanoparticles, a copper-based metal-organic framework and graphene oxide. The use of ML in this case was trained to learn the relation between creatinine concentrations in serum and in tears and gain the ability to discriminate between low, normal and high concentrations of creatinine in patients using a non-invasive method and a wearable device.

In another work from Kalasin et al. [167], a wearable pH sensor was used for wound monitoring. The potentiometric working electrode was based on polyaniline and cuprous oxide nanoparticles. The measured electrode potential was processed using ML and deep learning algorithms to predict wound healing stages (inflammatory, proliferative, remodelling). As expected, the deep learning algorithm performed better than tested ML algorithms. Interestingly, this sensor also included flexible electronics and a 13.56 MHz antenna for energy harvesting and sensor readout.

One common problem regarding electrochemical detection of multiple analytes and complex matrices is the superposition of signals and mutual interference. ML algorithms can be used for signal discrimination. For instance, a flexible electrode made from laser-induced graphene and molybdenum sulphide was fabricated and used for the simultaneous detection of tyrosine and uric acid in sweat and saliva [168]. In this case, various ML algorithms were trained using data from various electrochemical techniques, such as cyclic voltammetry, square wave voltammetry, differential pulse voltammetry, and large amplitude AC voltammetry. In this case, the application of ML algorithms was useful not only for the discrimination of both analytes but also for lowering the LOD to 100 nM and 10 nM for tyrosine and uric acid, respectively.

Regarding potentiometric simultaneous detection of ions in sweat, an emulator for providing data for training a ML algorithm was developed by Hanitra et al. [170]. This emulator was developed using, for the generation of simulated data, ion selective electrodes for Na⁺, K⁺, Li⁺, and Pb²⁺ at different mixed concentrations considering ion activities,

selectivity coefficients, and offset parameters extracted from real ISE calibration curves. This emulator was able to provide 10 datasets of 68 points for training ML algorithms of different complexity. In this work, a multivariate vector regression model performed equally accurately and much faster compared to a more computationally complex neural network.

ML algorithms are useful tools for enhancing the performance of electrochemical sweat sensors, especially ESSCMs. Their main application in sweat sensing is the classification of health status and prediction of abnormal analyte concentrations in a possible future event, rather than contributing to extremely accurate concentration measurement. Supervised learning algorithms are most used for applications for sweat electrochemical sensors. These algorithms are used in combination with other strategies, such as use of nanomaterials, multisensory approaches, and non-ML signal processing, to enhance their sensor accuracy, LOD, and ability for correct classification and prediction. Training data and computational availability are still a limitation regarding electrochemical sweat sensors at a research scale, but these limitations can be overcome once the sensors are used at a larger scale in combination with the internet of things and cloud computing.

8. Regulatory Aspects

According to the United States Food and Drug Administration (FDA) “General Wellness: Policy for Low-Risk Devices” guide, wearables should be considered medical devices if they are intended to diagnose or treat a health condition or disease. Wearable medical devices (WMDs), as any other medical devices, are regulated by health authorities over the entire life cycle to ensure their safety, efficacy, and constant quality level.

ISO 14971 (“Medical Devices: Application of risk management to medical devices”) is an FDA-recognized standard that provides medical device manufacturers with a framework to systematically manage the risks to people, property, and the environment associated with the use of medical devices. Risk management impacts the design and testing phases of the manufacturing process. Application of ISO 14971 helps to develop devices free of structural defects that could mean a risk to the patient or could compromise the correct technical functioning. Ravizza et al. [171] recognized as a main risk for WMDs software malfunction, hacking of data, loss or alteration of data, electrical hazards, and electromagnetic compatibility (IEC 60601), biocompatibility (ISO 10993), and physic and chemical stability.

Additionally, the FDA classifies WMDs according to their risk as low-risk Class I, moderated-risk Class II and high-risk Class III. Most WMDs can be considered Class I or Class II and require general or special controls, respectively. However, some products (e.g., wearable automated external defibrillators) are considered high-risk Class III WMDs and require premarket approval.

Before the manufacturing of medical devices, it is imperative to evaluate which materials will be used and their interactions with the human body. ISO 10993: “Biological evaluation of medical devices” intends to protect humans from potential biological risks from the use of medical devices. For a complete biological safety evaluation, it classifies medical devices according to the nature and duration of their contact with human tissues. According to ISO 10993, WMDs can be categorized as intact skin surface devices, which are indispensable for evaluating cytotoxicity, sensitization, and irritation or intracutaneous reactivity.

Polymers used in medical devices must be biocompatible; i.e., they must be able to be in contact with living systems without producing an adverse effect [38]. A list of the most used biocompatible polymers in flexible electronics is presented in Appendix A. [39,40]. Several authors have proposed the use of polydimethylsiloxane, a soft and non-irritating material often employed in microfluidic systems [69,172]. PDMS is soft and comfortable to wear for extended periods of time (at least 6 h) without causing skin irritation. Furthermore, PDMS prevents sensor chip bending when the sensing system is attached to slightly curved body parts, such as the upper torso (front or back) or upper limbs (arms or legs) [69].

Another commonly used substrate is fabric. Fibre sensors can be woven into a fabric, and compared with the traditional thin-film sensor, fabric sensors can bear various com-

plexes and even support severe deformations, such as twisting, while providing an effective and comfortable interface with human skin (i.e., the fabric is breathable and comfortable), and the sensor could be used for the long term without discomfort to users [67].

9. Concluding Remarks

The development of reliable electrochemical sweat sensors requires sensitive, highly selective detection of targets, the electrochemical transduction of which must be integrated into associated electronic circuits for signal processing and external communication. Many efforts have been directed in the biosensors community to attain lower LODs and higher sensitivity, along with an extended lifetime under working conditions. Many challenges must still be solved, especially regarding collecting representative sweat samples and improving signal processing in wearables, considering the signal drift due to sensor aging, interference, and noise introduced by the user. The processing of signals by machine learning could offer a new approach to improve the reliability of sweat sensors.

Author Contributions: Writing—original draft preparation, all authors; writing—review and editing, all authors; supervision, G.Y. All authors have read and agreed to the published version of the manuscript.

Funding: This research was funded by the Instituto Nacional de Tecnología Industrial (INTI), Argentina.

Conflicts of Interest: The authors declare no conflict of interest.

Appendix A

Polyethylene, cellulose, silk, shellac, polylactic acid, polycaprolactone, polyethylene glycol, albumen, polyglycerol-co-sebacate, polylactic-co-glycolic acid, polypropylene, polytetrafluoroethylene, polymethylmethacrylate, polyethylene-co-vinyl acetate, polydimethylsiloxane, low MW polydimethylsiloxane, polyether urethanes, polyethylene terephthalate, polysulphone, polyethylene oxide, polyethylene oxide co propylene oxide, polyvinyl alcohol, polyaniline, polypyrrole, poly(3,4 ethylenedioxythiophene), melanin, PDPP-DP, polyvinylidene fluoride.

References

1. Baker, L.B. Physiology of sweat gland function: The roles of sweating and sweat composition in human health. *Temperature* **2019**, *6*, 211–259. [[CrossRef](#)] [[PubMed](#)]
2. Qiao, Y.; Qiao, L.; Chen, Z.; Liu, B.; Gao, L.; Zhang, L. Wearable Sensor for Continuous Sweat Biomarker Monitoring. *Chemosensors* **2022**, *10*, 273. [[CrossRef](#)]
3. Van Hoovels, K.; Xuan, X.; Cuartero, M.; Gijssels, M.; Swarén, M.; Crespo, G.A. Can Wearable Sweat Lactate Sensors Contribute to Sports Physiology? *ACS Sens.* **2021**, *6*, 3496–3508. [[CrossRef](#)] [[PubMed](#)]
4. Gao, W.; Nyein, H.Y.Y.; Shahpar, Z.; Fahad, H.M.; Chen, K.; Emaminejad, S.; Gao, Y.; Tai, L.C.; Ota, H.; Wu, E.; et al. Wearable Microsensor Array for Multiplexed Heavy Metal Monitoring of Body Fluids. *ACS Sens.* **2016**, *1*, 866–874. [[CrossRef](#)]
5. Xu, J.; Fang, Y.; Chen, J. Wearable biosensors for non-invasive sweat diagnostics. *Biosensors* **2021**, *11*, 245. [[CrossRef](#)] [[PubMed](#)]
6. Gao, F.; Liu, C.; Zhang, L.; Liu, T.; Wang, Z.; Song, Z.; Cai, H.; Fang, Z.; Chen, J.; Wang, J.; et al. Wearable and flexible electrochemical sensors for sweat analysis: A review. *Microsyst. Nanoeng.* **2023**, *9*, 1. [[CrossRef](#)] [[PubMed](#)]
7. Gao, W.; Emaminejad, S.; Nyein, H.Y.Y.; Challa, S.; Chen, K.; Peck, A.; Fahad, H.M.; Ota, H.; Shiraki, H.; Kiriya, D.; et al. Fully integrated wearable sensor arrays for multiplexed in situ perspiration analysis. *Nature* **2016**, *529*, 509–514. [[CrossRef](#)]
8. Emaminejad, S.; Gao, W.; Wu, E.; Davies, Z.A.; Nyein, H.Y.Y.; Challa, S.; Ryan, S.P.; Fahad, H.M.; Chen, K.; Shahpar, Z.; et al. Autonomous sweat extraction and analysis applied to cystic fibrosis and glucose monitoring using a fully integrated wearable platform. *Proc. Natl. Acad. Sci. USA* **2017**, *114*, 4625–4630. [[CrossRef](#)]
9. Patterson, M.J.; Galloway, S.D.R.; Nimmo, M.A. Variations in regional sweat composition in normal human males. *Exp. Physiol.* **2000**, *85*, 869–875. [[CrossRef](#)]
10. Nyein, H.Y.Y.; Gao, W.; Shahpar, Z.; Emaminejad, S.; Challa, S.; Chen, K.; Fahad, H.M.; Tai, L.C.; Ota, H.; Davis, R.W.; et al. A Wearable Electrochemical Platform for Noninvasive Simultaneous Monitoring of Ca²⁺ and pH. *ACS Nano* **2016**, *10*, 7216–7224. [[CrossRef](#)]
11. Anastasova, S.; Crewther, B.; Bembnowicz, P.; Curto, V.; Ip, H.M.D.; Rosa, B.; Yang, G.-Z. A wearable multisensing patch for continuous sweat monitoring. *Biosens. Bioelectron.* **2017**, *93*, 139–145. [[CrossRef](#)] [[PubMed](#)]

12. Kim, J.; Jeerapan, I.; Imani, S.; Cho, T.N.; Bandodkar, A.; Cinti, S.; Mercier, P.P.; Wang, J. Noninvasive Alcohol Monitoring Using a Wearable Tattoo-Based Iontophoretic-Biosensing System. *ACS Sens.* **2016**, *1*, 1011–1019. [[CrossRef](#)]
13. Windmiller, J.R.; Bandodkar, A.J.; Valdés-Ramírez, G.; Parkhomovsky, S.; Martínez, A.G.; Wang, J. Electrochemical sensing based on printable temporary transfer tattoos. *Chem. Commun.* **2012**, *48*, 6794–6796. [[CrossRef](#)] [[PubMed](#)]
14. Kinnamon, D.; Ghanta, R.; Lin, K.C.; Muthukumar, S.; Prasad, S. Portable biosensor for monitoring cortisol in low-volume perspired human sweat. *Sci. Rep.* **2017**, *7*, 13312. [[CrossRef](#)]
15. Montón, E.; Hernandez, J.F.; Blasco, J.M.; Hervé, T.; Micallef, J.; Grech, I.; Brincat, A.; Traver, V. Body area network for wireless patient monitoring. *IET Commun.* **2008**, *2*, 215–222. [[CrossRef](#)]
16. LeGrys, V.A.; Yankaskas, J.R.; Quittell, L.M.; Marshall, B.C.; Mogayzel, P.J. Diagnostic Sweat Testing: The Cystic Fibrosis Foundation Guidelines. *J. Pediatr.* **2007**, *151*, 85–89. [[CrossRef](#)] [[PubMed](#)]
17. Moyer, J.; Wilson, D.; Finkelshtein, I.; Wong, B.; Potts, R. Correlation between sweat glucose and blood glucose in subjects with diabetes. *Diabetes Technol. Ther.* **2012**, *14*, 398–402. [[CrossRef](#)]
18. Xue, W.; Tan, X.; Khaing Oo, M.K.; Kulkarni, G.; Ilgen, M.A.; Fan, X. Rapid and sensitive detection of drugs of abuse in sweat by multiplexed capillary based immuno-biosensors. *Analyst* **2020**, *145*, 1346–1354. [[CrossRef](#)]
19. Tai, L.C.; Gao, W.; Chao, M.; Bariya, M.; Ngo, Q.P.; Shahpar, Z.; Nyein, H.Y.Y.; Park, H.; Sun, J.; Jung, Y.; et al. Methylxanthine Drug Monitoring with Wearable Sweat Sensors. *Adv. Mater.* **2018**, *30*, 1707442. [[CrossRef](#)]
20. Teymourian, H.; Parrilla, M.; Sempionatto, J.R.; Montiel, N.F.; Barfidokht, A.; Van Echelpoel, R.; De Wael, K.; Wang, J. Wearable Electrochemical Sensors for the Monitoring and Screening of Drugs. *ACS Sens.* **2020**, *5*, 2679–2700. [[CrossRef](#)]
21. Lam Po Tang, S. Wearable sensors for sports performance. In *Textiles for Sportswear*; Elsevier Inc.: Amsterdam, The Netherlands, 2015; pp. 169–196. ISBN 9781782422297.
22. Parrilla, M.; Ortiz-Gómez, I.; Cánovas, R.; Salinas-Castillo, A.; Cuartero, M.; Crespo, G.A. Wearable Potentiometric Ion Patch for On-Body Electrolyte Monitoring in Sweat: Toward a Validation Strategy to Ensure Physiological Relevance. *Anal. Chem.* **2019**, *91*, 8644–8651. [[CrossRef](#)] [[PubMed](#)]
23. Xuan, X.; Pérez-Ràfols, C.; Chen, C.; Cuartero, M.; Crespo, G.A. Lactate Biosensing for Reliable On-Body Sweat Analysis. *ACS Sens.* **2021**, *6*, 2763–2771. [[CrossRef](#)] [[PubMed](#)]
24. Zhang, L.; Liu, J.; Fu, Z.; Qi, L. A Wearable Biosensor Based on Bienzyme Gel-Membrane for Sweat Lactate Monitoring by Mounting on Eyeglasses. *J. Nanosci. Nanotechnol.* **2020**, *20*, 1495–1503. [[CrossRef](#)] [[PubMed](#)]
25. Liu, C.; Xu, T.; Wang, D.; Zhang, X. The role of sampling in wearable sweat sensors. *Talanta* **2020**, *212*, 120801. [[CrossRef](#)] [[PubMed](#)]
26. Bae, C.W.; Chinnamani, M.V.; Lee, E.H.; Lee, N.E. Stretchable Non-Enzymatic Fuel Cell-Based Sensor Patch Integrated with Thread-Embedded Microfluidics for Self-Powered Wearable Glucose Monitoring. *Adv. Mater. Interfaces* **2022**, *9*, 2200492. [[CrossRef](#)]
27. Sharma, A.; Singh, A.; Gupta, V.; Arya, S. Advancements and future prospects of wearable sensing technology for healthcare applications. *Sens. Diagn.* **2022**, *1*, 387–404. [[CrossRef](#)]
28. Sharma, A.; Badea, M.; Tiwari, S.; Marty, J.L. Wearable biosensors: An alternative and practical approach in healthcare and disease monitoring. *Molecules* **2021**, *26*, 748. [[CrossRef](#)]
29. Kim, J.; Sempionatto, J.R.; Imani, S.; Hartel, M.C.; Barfidokht, A.; Tang, G.; Campbell, A.S.; Mercier, P.P.; Wang, J. Simultaneous Monitoring of Sweat and Interstitial Fluid Using a Single Wearable Biosensor Platform. *Adv. Sci.* **2018**, *5*, 14–23. [[CrossRef](#)]
30. Li, M.; Wang, L.; Liu, R.; Li, J.; Zhang, Q.; Shi, G.; Li, Y.; Hou, C.; Wang, H. A highly integrated sensing paper for wearable electrochemical sweat analysis. *Biosens. Bioelectron.* **2021**, *174*, 112828. [[CrossRef](#)]
31. He, X.; Xu, T.; Gu, Z.; Gao, W.; Xu, L.P.; Pan, T.; Zhang, X. Flexible and Superwetable Bands as a Platform toward Sweat Sampling and Sensing. *Anal. Chem.* **2019**, *91*, 4296–4300. [[CrossRef](#)]
32. Dai, B.; Li, K.; Shi, L.; Wan, X.; Liu, X.; Zhang, F.; Jiang, L.; Wang, S. Bioinspired Janus Textile with Conical Micropores for Human Body Moisture and Thermal Management. *Adv. Mater.* **2019**, *31*, 1904113. [[CrossRef](#)]
33. Cao, Q.; Liang, B.; Tu, T.; Wei, J.; Fang, L.; Ye, X. Three-dimensional paper-based microfluidic electrochemical integrated devices (3D-PMED) for wearable electrochemical glucose detection. *RSC Adv.* **2019**, *9*, 5674–5681. [[CrossRef](#)]
34. Sophocleous, M.; Atkinson, J.K. A review of screen-printed silver/silver chloride (Ag/AgCl) reference electrodes potentially suitable for environmental potentiometric sensors. *Sens. Actuators A Phys.* **2017**, *267*, 106–120. [[CrossRef](#)]
35. Bandodkar, A.J.; Jeang, W.J.; Ghaffari, R.; Rogers, J.A. Wearable Sensors for Biochemical Sweat Analysis. *Annu. Rev. Anal. Chem.* **2019**, *12*, 201–224. [[CrossRef](#)]
36. Kumar, A.K.S.; Zhang, Y.; Li, D.; Compton, R.G. A mini-review: How reliable is the drop casting technique? *Electrochem. Commun.* **2020**, *121*, 106867. [[CrossRef](#)]
37. Suresh, R.R.; Lakshmanakumar, M.; Arockia Jayalatha, J.B.B.; Rajan, K.S.; Sethuraman, S.; Krishnan, U.M.; Rayappan, J.B.B. Fabrication of screen-printed electrodes: Opportunities and challenges. *J. Mater. Sci.* **2021**, *56*, 8951–9006. [[CrossRef](#)]
38. Gan, S.; Liao, C.; Liang, R.; Du, S.; Zhong, L.; Tang, Y.; Han, T.; Bao, Y.; Sun, Z.; Ma, Y.; et al. A Solid-Contact Reference Electrode Based on Silver/Silver Organic Insoluble Salt for Potentiometric Ion Sensing. *ACS Meas. Sci. Au* **2022**, *2*, 568–575. [[CrossRef](#)]
39. Dawkins, R.C.; Wen, D.; Hart, J.N.; Vepsäläinen, M. A screen-printed Ag/AgCl reference electrode with long-term stability for electroanalytical applications. *Electrochim. Acta* **2021**, *393*, 139043. [[CrossRef](#)]

40. Macedo, D.S.; Vepsäläinen, M.; Acharya, D.; Wood, C.D.; Wen, D.; Thomson, L.; Peacock, S.; Rodopoulos, T.; Hogan, C.F. An unusually stable solid state Ag|AgCl reference electrode for long term continuous measurements based on a crosslinked poly(vinyl acetate)/KCl composite. *Electrochim. Acta* **2021**, *368*, 137636. [[CrossRef](#)]
41. Moya, A.; Pol, R.; Martínez-Cuadrado, A.; Villa, R.; Gabriel, G.; Baeza, M. Stable Full-Inkjet-Printed Solid-State Ag/AgCl Reference Electrode. *Anal. Chem.* **2019**, *91*, 15539–15546. [[CrossRef](#)]
42. Komoda, M.; Shitanda, I.; Hoshi, Y.; Itagaki, M. Fabrication and characterization of a fully screen-printed Ag/AgCl reference electrode using silica gel inks exhibiting instantaneous usability and long-term stability. *Electrochemistry* **2019**, *87*, 65–69. [[CrossRef](#)]
43. Manjakkal, L.; Shakthivel, D.; Dahiya, R. Flexible Printed Reference Electrodes for Electrochemical Applications. *Adv. Mater. Technol.* **2018**, *3*, 1800252. [[CrossRef](#)]
44. Wang, S.; Wu, Y.; Gu, Y.; Li, T.; Luo, H.; Li, L.-H.; Bai, Y.; Li, L.; Liu, L.; Cao, Y.; et al. Wearable Sweatband Sensor Platform Based on Gold Nanodendrite Array as Efficient Solid Contact of Ion-Selective Electrode. *Anal. Chem.* **2017**, *89*, 10224–10231. [[CrossRef](#)]
45. Alva, S.; Heng, L.Y.; Ahmad, M. Optimization of Screen Printed Reference Electrode Based on Charge Balance and Poly (Butyl Acrylate) Photocurable Membrane. *Int. J. Innov. Mech. Eng. Adv. Mater.* **2016**, *2*, 10. [[CrossRef](#)]
46. Tangkuaram, T.; Ponchio, C.; Kangkasomboon, T.; Katikawong, P.; Veerasai, W. Design and development of a highly stable hydrogen peroxide biosensor on screen printed carbon electrode based on horseradish peroxidase bound with gold nanoparticles in the matrix of chitosan. *Biosens. Bioelectron.* **2007**, *22*, 2071–2078. [[CrossRef](#)]
47. Guan, W.-J.; Li, Y.; Chen, Y.-Q.; Zhang, X.-B.; Hu, G.-Q. Glucose biosensor based on multi-wall carbon nanotubes and screen printed carbon electrodes. *Biosens. Bioelectron.* **2005**, *21*, 508–512. [[CrossRef](#)]
48. Guinovart, T.; Crespo, G.A.; Rius, F.X.; Andrade, F.J. A reference electrode based on polyvinyl butyral (PVB) polymer for decentralized chemical measurements. *Anal. Chim. Acta* **2014**, *821*, 72–80. [[CrossRef](#)]
49. Parrilla, M.; Ferré, J.; Guinovart, T.; Andrade, F.J. Wearable Potentiometric Sensors Based on Commercial Carbon Fibres for Monitoring Sodium in Sweat. *Electroanalysis* **2016**, *28*, 1267–1275. [[CrossRef](#)]
50. Bananezhad, A.; Jović, M.; Villalobos, L.F.; Agrawal, K.V.; Ganjali, M.R.; Girault, H.H. Large-scale fabrication of flexible solid-state reference electrodes. *J. Electroanal. Chem.* **2019**, *847*, 113241. [[CrossRef](#)]
51. Veiga, L.S.; Garate, O.; Giménez, G.; Ybarra, G.; Monsalve, L.N. *Nanomaterial-Based Multifunctional Inks for the Fabrication of Printed Biosensors*, 1st ed.; Gupta, R.K., Nguyen, T., Eds.; Elsevier: Amsterdam, The Netherlands, 2022; ISBN 9780323911450.
52. Lou, S.; Chen, Q.; Wang, W.; Wang, Y.; Zhou, S. Template-assisted synthesis of Ag/AgCl hollow microcubes and their composition-dependent photocatalytic activity for the degradation of phenol. *RSC Adv.* **2021**, *11*, 26311–26318. [[CrossRef](#)]
53. Bieg, C.; Fuchsberger, K.; Stelzle, M. Introduction to polymer-based solid-contact ion-selective electrodes—Basic concepts, practical considerations, and current research topics. *Anal. Bioanal. Chem.* **2017**, *409*, 45–61. [[CrossRef](#)]
54. Bilbao, E.; Kapadia, S.; Riechert, V.; Amalvy, J.; Molinari, F.N.; Escobar, M.M.; Baumann, R.R.; Monsalve, L.N. Functional aqueous-based polyaniline inkjet inks for fully printed high-performance pH-sensitive electrodes. *Sens. Actuators B Chem.* **2021**, *346*, 130558. [[CrossRef](#)]
55. Kumar, P.A.; Pradeep, A.; Nair, B.K.G.; Babu, T.G.S.; Suneesh, P.V. Silver-manganese nanocomposite modified screen-printed carbon electrode in the fabrication of an electrochemical, disposable biosensor strip for cystic fibrosis. *Microchim. Acta* **2022**, *189*, 327. [[CrossRef](#)]
56. Cui, X.; Bao, Y.; Han, T.; Liu, Z.; Ma, Y.; Sun, Z. A wearable electrochemical sensor based on β -CD functionalized graphene for pH and potassium ion analysis in sweat. *Talanta* **2022**, *245*, 123481. [[CrossRef](#)]
57. Ozer, T.; Agir, I.; Henry, C.S. Low-cost Internet of Things (IoT)-enabled a wireless wearable device for detecting potassium ions at the point of care. *Sens. Actuators B Chem.* **2022**, *365*, 131961. [[CrossRef](#)]
58. Wang, S.; Liu, M.; Shi, Y.; Yang, X.; Li, L.; Lu, Q.; Zheng, H.; Feng, S.; Bai, Y.; Zhang, T. Vertically aligned conductive metal-organic framework nanowires array composite fiber as efficient solid-contact for wearable potentiometric sweat sensing. *Sens. Actuators B Chem.* **2022**, *369*, 132290. [[CrossRef](#)]
59. Yeung, K.K.; Li, J.; Huang, T.; Hosseini, I.I.; Al Mahdi, R.; Alam, M.M.; Sun, H.; Mahshid, S.; Yang, J.; Ye, T.T.; et al. Utilizing Gradient Porous Graphene Substrate as the Solid-Contact Layer To Enhance Wearable Electrochemical Sweat Sensor Sensitivity. *Nano Lett.* **2022**, *22*, 6647–6654. [[CrossRef](#)]
60. Iannazzo, D.; Espro, C.; Ferlazzo, A.; Celesti, C.; Branca, C.; Neri, G. Electrochemical and fluorescent properties of crown ether functionalized graphene quantum dots for potassium and sodium ions detection. *Nanomaterials* **2021**, *11*, 2897. [[CrossRef](#)] [[PubMed](#)]
61. Napier, B.S.; Matzeu, G.; Lo Presti, M.; Omenetto, F.G. Dry Spun, Bulk-Functionalized rGO Fibers for Textile Integrated Potentiometric Sensors. *Adv. Mater. Technol.* **2022**, *7*, 2101508. [[CrossRef](#)]
62. Liao, J.; Zhang, X.; Sun, Z.; Chen, H.; Fu, J.; Si, H.; Ge, C.; Lin, S. Laser-Induced Graphene-Based Wearable Epidermal Ion-Selective Sensors for Noninvasive Multiplexed Sweat Analysis. *Biosensors* **2022**, *12*, 397. [[CrossRef](#)] [[PubMed](#)]
63. Ghoorchian, A.; Kamalabadi, M.; Moradi, M.; Madrakian, T.; Afkhami, A.; Bagheri, H.; Ahmadi, M.; Khoshsafar, H. Wearable Potentiometric Sensor Based on Na_{0.44}MnO₂ for Non-invasive Monitoring of Sodium Ions in Sweat. *Anal. Chem.* **2022**, *94*, 2263–2270. [[CrossRef](#)]
64. Jiang, T.; Yin, B.; Liu, X.; Yang, L.; Pang, H.; Song, J.; Wu, S. Porous carbon-based robust, durable, and flexible electrochemical device for K⁺ detection in sweat†. *Analyst* **2022**, *147*, 1144–1151. [[CrossRef](#)]

65. Sempionatto, J.R.; Nakagawa, T.; Pavinatto, A.; Mensah, S.T.; Imani, S.; Mercier, P.; Wang, J. Eyeglasses based wireless electrolyte and metabolite sensor platform. *Lab Chip* **2017**, *17*, 1834–1842. [[CrossRef](#)] [[PubMed](#)]
66. Moina, C.; Ybarra, G. Fundamentals and applications of immunosensors. In *Advances in Immunoassay Technology*; Theodore, K., Chiu, N., Eds.; InTech: Zagreb, Croatia, 2012; pp. 65–80.
67. Wang, L.; Wang, L.; Zhang, Y.; Pan, J.; Li, S.; Sun, X.; Zhang, B.; Peng, H. Weaving Sensing Fibers into Electrochemical Fabric for Real-Time Health Monitoring. *Adv. Funct. Mater.* **2018**, *28*, 1804456. [[CrossRef](#)]
68. Jiang, D.; Xu, C.; Zhang, Q.; Ye, Y.; Cai, Y.; Li, K.; Li, Y.; Huang, X.; Wang, Y. In-situ preparation of lactate-sensing membrane for the noninvasive and wearable analysis of sweat. *Biosens. Bioelectron.* **2022**, *210*, 114303. [[CrossRef](#)] [[PubMed](#)]
69. Shitanda, I.; Mitsumoto, M.; Loew, N.; Yoshihara, Y.; Watanabe, H.; Mikawa, T.; Tsujimura, S.; Itagaki, M.; Motosuke, M. Continuous sweat lactate monitoring system with integrated screen-printed Mgo-templated carbon-lactate oxidase biosensor and microfluidic sweat collector. *Electrochim. Acta* **2021**, *368*, 137620. [[CrossRef](#)]
70. Tai, L.C.; Liaw, T.S.; Lin, Y.; Nyein, H.Y.Y.; Bariya, M.; Ji, W.; Hettick, M.; Zhao, C.; Zhao, J.; Hou, L.; et al. Wearable Sweat Band for Noninvasive Levodopa Monitoring. *Nano Lett.* **2019**, *19*, 6346–6351. [[CrossRef](#)] [[PubMed](#)]
71. Adachi, T.; Kitazumi, Y.; Shirai, O.; Kano, K. Direct Electron Transfer-Type Bioelectrocatalysis of Redox Enzymes at Nanostructured Electrodes. *Catalysts* **2020**, *10*, 236. [[CrossRef](#)]
72. Hojaiji, H.; Zhao, Y.; Gong, M.C.; Mallajosyula, M.; Tan, J.; Lin, H.; Hojaiji, A.M.; Lin, S.; Milla, C.; Madni, A.M.; et al. An autonomous wearable system for diurnal sweat biomarker data acquisition. *Lab Chip* **2020**, *20*, 4582–4591. [[CrossRef](#)] [[PubMed](#)]
73. Sempionatto, J.R.; Khorshed, A.A.; Ahmed, A.; De Loyola E Silva, A.N.; Barfidokht, A.; Yin, L.; Goud, K.Y.; Mohamed, M.A.; Bailey, E.; May, J.; et al. Epidermal Enzymatic Biosensors for Sweat Vitamin C: Toward Personalized Nutrition. *ACS Sens.* **2020**, *5*, 1804–1813. [[CrossRef](#)] [[PubMed](#)]
74. Wang, Y.X.; Rinawati, M.; De Zhan, J.; Lin, K.Y.; Huang, C.J.; Chen, K.J.; Mizuguchi, H.; Jiang, J.C.; Hwang, B.J.; Yeh, M.H. Boron-Doped Graphene Quantum Dots Anchored to Carbon Nanotubes as Noble Metal-Free Electrocatalysts of Uric Acid for a Wearable Sweat Sensor. *ACS Appl. Nano Mater.* **2022**, *5*, 11100–11110. [[CrossRef](#)]
75. Jang, J.H.; Lim, H.B. Characterization and analytical application of surface modified magnetic nanoparticles. *Microchem. J.* **2010**, *94*, 148–158. [[CrossRef](#)]
76. Migneault, I.; Dartiguenave, C.; Bertrand, M.J.; Waldron, K.C. Glutaraldehyde: Behavior in aqueous solution, reaction with proteins, and application to enzyme crosslinking. *Biotechniques* **2004**, *37*, 790–802. [[CrossRef](#)]
77. Sassolas, A.; Blum, L.J.; Leca-Bouvier, B.D. Immobilization strategies to develop enzymatic biosensors. *Biotechnol. Adv.* **2012**, *30*, 489–511. [[CrossRef](#)]
78. Grieshaber, D.; MacKenzie, R.; Vörös, J.; Reimhult, E. Electrochemical Biosensors—Sensor Principles and Architectures. *Sensors* **2008**, *8*, 1400–1458. [[CrossRef](#)]
79. Economou, A.; Karapetis, S.K.; Nikoleli, G.-P.; Nikolelis, D.P.; Bratakou, S.; Varzakas, T.H. Enzyme-based Sensors. In *Advances in Food Diagnostics*; Toldrá, F., Nollet, L.M.L., Eds.; John Wiley & Sons Ltd.: Hoboken, NJ, USA, 2017; pp. 231–250, ISBN 9781119105916.
80. Sonawane, A.; Manickam, P.; Bhansali, S. Stability of Enzymatic Biosensors for Wearable Applications. *IEEE Rev. Biomed. Eng.* **2017**, *10*, 174–186. [[CrossRef](#)]
81. Balcão, V.M.; Vila, M.M.D.C. Structural and functional stabilization of protein entities: State-of-the-art. *Adv. Drug Deliv. Rev.* **2015**, *93*, 25–41. [[CrossRef](#)]
82. Garcia-Galan, C.; Berenguer-Murcia, Á.; Fernandez-Lafuente, R.; Rodrigues, R.C. Potential of different enzyme immobilization strategies to improve enzyme performance. *Adv. Synth. Catal.* **2011**, *353*, 2885–2904. [[CrossRef](#)]
83. Rathee, K.; Dhull, V.; Dhull, R.; Singh, S. Biosensors based on electrochemical lactate detection: A comprehensive review. *Biochem. Biophys. Rep.* **2016**, *5*, 35–54. [[CrossRef](#)]
84. Thévenot, D.R.; Toth, K.; Durst, R.A.; Wilson, G.S. Electrochemical biosensors: Recommended definitions and classification. *Biosens. Bioelectron.* **2001**, *16*, 121–131. [[CrossRef](#)] [[PubMed](#)]
85. Cunha-Silva, H.; Pires, F.; Dias-Cabral, A.C.; Arcos-Martinez, M.J. Inhibited enzymatic reaction of crosslinked lactate oxidase through a pH-dependent mechanism. *Colloids Surf. B Biointerfaces* **2019**, *184*, 110490. [[CrossRef](#)]
86. Klimuntowski, M.; Alam, M.M.; Singh, G.; Howlader, M.M.R. Electrochemical Sensing of Cannabinoids in Biofluids: A Noninvasive Tool for Drug Detection. *ACS Sens.* **2020**, *5*, 620–636. [[CrossRef](#)] [[PubMed](#)]
87. Saldanha, D.J.; Cai, A.; Dorval Courchesne, N.M. The Evolving Role of Proteins in Wearable Sweat Biosensors. *ACS Biomater. Sci. Eng.* **2021**; Article in press. [[CrossRef](#)]
88. Santiago, E.; Poudyal, S.S.; Shin, S.Y.; Yoon, H.J. Graphene Oxide Functionalized Biosensor for Detection of Stress-Related Biomarkers. *Sensors* **2022**, *22*, 558. [[CrossRef](#)]
89. Laochai, T.; Yukird, J.; Promphet, N.; Qin, J.; Chailapakul, O.; Rodthongkum, N. Non-invasive electrochemical immunosensor for sweat cortisol based on L-cys/AuNPs/MXene modified thread electrode. *Biosens. Bioelectron.* **2022**, *203*, 114039. [[CrossRef](#)]
90. Madhu, S.; Anthuuvan, A.J.; Ramasamy, S.; Manickam, P.; Bhansali, S.; Nagamony, P.; Chinnuswamy, V. ZnO Nanorod Integrated Flexible Carbon Fibers for Sweat Cortisol Detection. *ACS Appl. Electron. Mater.* **2020**, *2*, 499–509. [[CrossRef](#)]
91. Madhu, S.; Ramasamy, S.; Manickam, P.; Nagamony, P.; Chinnuswamy, V. TiO₂ anchored carbon fibers as non-invasive electrochemical sensor platform for the cortisol detection. *Mater. Lett.* **2022**, *308*, 131238. [[CrossRef](#)]

92. Naik, A.R.; Zhou, Y.; Dey, A.A.; Arellano, D.L.G.; Okoroanyanwu, U.; Secor, E.B.; Hersam, M.C.; Morse, J.; Rothstein, J.P.; Carter, K.R.; et al. Printed microfluidic sweat sensing platform for cortisol and glucose detection. *Lab Chip* **2022**, *22*, 156–169. [CrossRef]
93. Nah, J.S.; Barman, S.C.; Zahed, M.A.; Sharifuzzaman, M.; Yoon, H.; Park, C.; Yoon, S.; Zhang, S.; Park, J.Y. A wearable microfluidics-integrated impedimetric immunosensor based on Ti_3C_2Tx MXene incorporated laser-burned graphene for noninvasive sweat cortisol detection. *Sens. Actuators B Chem.* **2021**, *329*, 129206. [CrossRef]
94. Cheng, C.; Li, X.; Xu, G.; Lu, Y.; Low, S.S.; Liu, G.; Zhu, L.; Li, C.; Liu, Q. Battery-free, wireless, and flexible electrochemical patch for in situ analysis of sweat cortisol via near field communication. *Biosens. Bioelectron.* **2021**, *172*, 112782. [CrossRef]
95. Ganguly, A.; Lin, K.C.; Muthukumar, S.; Prasad, S. Autonomous, Real-Time Monitoring Electrochemical Aptasensor for Circadian Tracking of Cortisol Hormone in Sub-microliter Volumes of Passively Eluted Human Sweat. *ACS Sens.* **2021**, *6*, 63–72. [CrossRef] [PubMed]
96. Demuru, S.; Kim, J.; El Chazli, M.; Bruce, S.; Dupertuis, M.; Binz, P.A.; Saubade, M.; Lafaye, C.; Briand, D. Antibody-Coated Wearable Organic Electrochemical Transistors for Cortisol Detection in Human Sweat. *ACS Sens.* **2022**, *6*, 16472–16475. [CrossRef]
97. Bariya, M.; Nyein, H.Y.Y.; Javey, A. Wearable sweat sensors. *Nat. Electron.* **2018**, *1*, 160–171. [CrossRef]
98. Guk, K.; Han, G.; Lim, J.; Jeong, K.; Kang, T.; Lim, E.K.; Jung, J. Evolution of wearable devices with real-time disease monitoring for personalized healthcare. *Nanomaterials* **2019**, *9*, 813. [CrossRef]
99. Ling, Y.; An, T.; Yap, L.W.; Zhu, B.; Gong, S.; Cheng, W. Disruptive, Soft, Wearable Sensors. *Adv. Mater.* **2020**, *32*, 1904664. [CrossRef]
100. Brothers, M.C.; Debrosse, M.; Grigsby, C.C.; Naik, R.R.; Hussain, S.M.; Heikenfeld, J.; Kim, S.S. Achievements and Challenges for Real-Time Sensing of Analytes in Sweat within Wearable Platforms. *Acc. Chem. Res.* **2019**, *52*, 297–306. [CrossRef]
101. Swetha, P.; Balijapalli, U.; Feng, S.P. Wireless accessing of salivary biomarkers based wearable electrochemical sensors: A mini-review. *Electrochem. Commun.* **2022**, *140*, 107314. [CrossRef]
102. Hong, Y.J.; Lee, H.; Kim, J.; Lee, M.; Choi, H.J.; Hyeon, T.; Kim, D.H. Multifunctional Wearable System that Integrates Sweat-Based Sensing and Vital-Sign Monitoring to Estimate Pre-/Post-Exercise Glucose Levels. *Adv. Funct. Mater.* **2018**, *28*, 1805754. [CrossRef]
103. Kim, J.; Campbell, A.S.; de Ávila, B.E.F.; Wang, J. Wearable biosensors for healthcare monitoring. *Nat. Biotechnol.* **2019**, *37*, 389–406. [CrossRef]
104. Colburn, A.W.; Levey, K.J.; O'Hare, D.; Macpherson, J.V. Lifting the lid on the potentiostat: A beginner's guide to understanding electrochemical circuitry and practical operation. *Phys. Chem. Chem. Phys.* **2021**, *23*, 8100–8117. [CrossRef]
105. Metrohm. Portable Potentiostats/Galvanostats. Available online: <https://www.metrohm.com/en/products/electrochemistry/portable-line.html> (accessed on 23 December 2022).
106. PalmSens. Available online: <https://www.palmsens.com/product-select/> (accessed on 1 April 2023).
107. Ivium. Available online: <https://www.ivium.com/> (accessed on 1 April 2023).
108. Irving, P.; Cecil, R.; Yates, M.Z. MYSTAT: A compact potentiostat/galvanostat for general electrochemistry measurements. *HardwareX* **2021**, *9*, e00163. [CrossRef]
109. Ainla, A.; Mousavi, M.P.S.; Tsaloglou, M.N.; Redston, J.; Bell, J.G.; Fernández-Abedul, M.T.; Whitesides, G.M. Open-Source Potentiostat for Wireless Electrochemical Detection with Smartphones. *Anal. Chem.* **2018**, *90*, 6240–6246. [CrossRef] [PubMed]
110. Dobbelaere, T.; Vereecken, P.M.; Detavernier, C. A USB-controlled potentiostat/galvanostat for thin-film battery characterization. *HardwareX* **2017**, *2*, 34–49. [CrossRef]
111. Dryden, M.D.M.; Wheeler, A.R. DStat: A versatile, open-source potentiostat for electroanalysis and integration. *PLoS ONE* **2015**, *10*, e0140349. [CrossRef] [PubMed]
112. Rowe, A.A.; Bonham, A.J.; White, R.J.; Zimmer, M.P.; Yadgar, R.J.; Hobza, T.M.; Honea, J.W.; Ben-Yaacov, I.; Plaxco, K.W. Cheapstat: An open-source, “do-it-yourself” potentiostat for analytical and educational applications. *PLoS ONE* **2011**, *6*, e23783. [CrossRef]
113. Tahernia, M.; Mohammadifar, M.; Liu, L.; Choi, S. A Disposable, Papertronic Three-Electrode Potentiostat for Monitoring Bacterial Electrochemical Activity. *ACS Omega* **2020**, *5*, 24717–24723. [CrossRef] [PubMed]
114. Alves, M.; Santos, Q. A Wearable Cortisol Monitoring Microsystem. Ph.D. Thesis, Universidade do Porto (Portugal), Porto, Portugal, 2021.
115. Hoilett, O.S.; Walker, J.F.; Balash, B.M.; Jaras, N.J.; Boppana, S.; Linnes, J.C. Kickstat: A coin-sized potentiostat for high-resolution electrochemical analysis. *Sensors* **2020**, *20*, 2407. [CrossRef] [PubMed]
116. Lin, H.; Tan, J.; Zhu, J.; Lin, S.; Zhao, Y.; Yu, W.; Hojajji, H.; Wang, B.; Yang, S.; Cheng, X.; et al. A programmable epidermal microfluidic valving system for wearable biofluid management and contextual biomarker analysis. *Nat. Commun.* **2020**, *11*, 4405. [CrossRef]
117. Texas Instruments. LMP91000. Available online: <https://www.ti.com/product/LMP91000> (accessed on 1 April 2023).
118. Brown, E.W.; Glasscott, M.W.; Conley, K.; Barr, J.; Ray, J.D.; Moores, L.C.; Netchaev, A. ACEstat: A DIY Guide to Unlocking the Potential of Integrated Circuit Potentiostats for Open-Source Electrochemical Analysis. *Anal. Chem.* **2022**, *94*, 4906–4912. [CrossRef]
119. Mintah Churcher, N.K.; Upasham, S.; Rice, P.; Bhadsavle, S.; Prasad, S. Development of a flexible, sweat-based neuropeptide y detection platform. *RSC Adv.* **2020**, *10*, 23173–23186. [CrossRef]

120. Analog Devices. ADuCM355. Available online: <https://www.analog.com/en/products/ADUCM355.html#product-overview> (accessed on 1 April 2023).
121. Analog Devices. AD5933. Available online: <https://www.analog.com/en/products/ad5933.html> (accessed on 1 April 2023).
122. Burgos-Flórez, F.; Rodríguez, A.; Cervera, E.; Zucolotto, V.; Sanjuán, M.; Villalba, P.J. TBISTAT: An open-source, wireless portable, electrochemical impedance spectroscopy capable potentiostat for the point-of-care detection of S100B in plasma samples. *PLoS ONE* **2022**, *17*, e0263738. [[CrossRef](#)]
123. Jenkins, D.M.; Lee, B.E.; Jun, S.; Reyes-De-Corcuera, J.; McLamore, E.S. ABE-Stat, a Fully Open-Source and Versatile Wireless Potentiostat Project Including Electrochemical Impedance Spectroscopy. *J. Electrochem. Soc.* **2019**, *166*, B3056–B3065. [[CrossRef](#)]
124. Vinoth, R.; Nakagawa, T.; Mathiyarasu, J.; Mohan, A.M.V. Fully Printed Wearable Microfluidic Devices for High-Throughput Sweat Sampling and Multiplexed Electrochemical Analysis. *ACS Sens.* **2021**, *6*, 1174–1186. [[CrossRef](#)]
125. Nag, A.; Mukhopadhyay, S.C.; Kosel, J. Wearable Flexible Sensors: A Review. *IEEE Sens. J.* **2017**, *17*, 3949–3960. [[CrossRef](#)]
126. Bandodkar, A.J.; Jeerapan, I.; Wang, J. Wearable Chemical Sensors: Present Challenges and Future Prospects. *ACS Sens.* **2016**, *1*, 464–482. [[CrossRef](#)]
127. Krorakai, K.; Klangphukhiew, S.; Kulchat, S.; Patramanon, R. Smartphone-based nfc potentiostat for wireless electrochemical sensing. *Appl. Sci.* **2021**, *11*, 392. [[CrossRef](#)]
128. Bandodkar, A.J.; Gutruf, P.; Choi, J.; Lee, K.; Sekine, Y.; Reeder, J.T.; Jeang, W.J.; Aranyosi, A.J.; Lee, S.P.; Model, J.B.; et al. Battery-free, skin-interfaced microfluidic/electronic systems for simultaneous electrochemical, colorimetric, and volumetric analysis of sweat. *Sci. Adv.* **2019**, *5*, eaav3294. [[CrossRef](#)]
129. Kim, B.J.; Kim, D.H.; Lee, Y.Y.; Shin, H.W.; Han, G.S.; Hong, J.S.; Mahmood, K.; Ahn, T.K.; Joo, Y.C.; Hong, K.S.; et al. Highly efficient and bending durable perovskite solar cells: Toward a wearable power source. *Energy Environ. Sci.* **2015**, *8*, 916–921. [[CrossRef](#)]
130. Bandodkar, A.J.; Molinnus, D.; Mirza, O.; Guinovart, T.; Windmiller, J.R.; Valdés-Ramírez, G.; Andrade, F.J.; Schöning, M.J.; Wang, J. Epidermal tattoo potentiometric sodium sensors with wireless signal transduction for continuous non-invasive sweat monitoring. *Biosens. Bioelectron.* **2014**, *54*, 603–609. [[CrossRef](#)]
131. Gai, Y.; Wang, E.; Liu, M.; Xie, L.; Bai, Y.; Yang, Y.; Xue, J.; Qu, X.; Xi, Y.; Li, L.; et al. A Self-Powered Wearable Sensor for Continuous Wireless Sweat Monitoring. *Small Methods* **2022**, *6*, 2200653. [[CrossRef](#)]
132. Song, Y.; Min, J.; Yu, Y.; Wang, H.; Yang, Y.; Zhang, H.; Gao, W. Wireless battery-free wearable sweat sensor powered by human motion. *Sci. Adv.* **2020**, *6*, eaay9842. [[CrossRef](#)]
133. Zheng, Y.; Yang, Y.; Chen, S.; Yuan, Q. Smart, stretchable and wearable supercapacitors: Prospects and challenges. *CrystEngComm* **2016**, *18*, 4218–4235. [[CrossRef](#)]
134. Xu, S.; Zhang, Y.; Cho, J.; Lee, J.; Huang, X.; Jia, L.; Fan, J.A.; Su, Y.; Su, J.; Zhang, H.; et al. Stretchable batteries with self-similar serpentine interconnects and integrated wireless recharging systems. *Nat. Commun.* **2013**, *4*, 1543. [[CrossRef](#)] [[PubMed](#)]
135. Kong, L.; Tang, C.; Peng, H.; Huang, J.; Zhang, Q. Advanced energy materials for flexible batteries in energy storage: A review. *SmartMat* **2020**, *1*, e1007. [[CrossRef](#)]
136. Kong, T.; Flanigan, S.; Weinstein, M.; Kalwa, U.; Legner, C.; Pandey, S. A fast, reconfigurable flow switch for paper microfluidics based on selective wetting of folded paper actuator strips. *Lab Chip* **2017**, *17*, 3621–3633. [[CrossRef](#)] [[PubMed](#)]
137. Nemiroski, A.; Christodouleas, D.C.; Hennek, J.W.; Kumar, A.A.; Maxwell, E.J.; Fernández-Abedul, M.T.; Whitesides, G.M. Universal mobile electrochemical detector designed for use in resource-limited applications. *Proc. Natl. Acad. Sci. USA* **2014**, *111*, 11984–11989. [[CrossRef](#)]
138. Rodríguez, Y.A. (Ed.) *2017 IEEE Colombian Conference on Communications and Computing (COLCOM)*; Conference Proceedings, 16–18 August 2017, Cartagena, Colombia; Institute of Electrical and Electronics Engineers Inc.: Piscataway, NJ, USA, 2017; ISBN 9781538610602.
139. Zhang, T.; Lu, J.; Hu, F.; Hao, Q. Bluetooth low energy for wearable sensor-based healthcare systems. In Proceedings of the 2014 IEEE Healthcare Innovation Conference (HIC), Seattle, WA, USA, 8–10 October 2014; Institute of Electrical and Electronics Engineers Inc.: Piscataway, NJ, USA, 2014; pp. 251–254.
140. Kovalska, E.; Baldycheva, A.; Somov, A. Wireless graphene-enabled wearable temperature sensor. In *Proceedings of the Journal of Physics: Conference Series*; IOP Publishing Ltd.: Bristol, UK, 2020; Volume 1571.
141. Bianchi, V.; Ciampolini, P.; De Munari, I. RSSI-Based Indoor Localization and Identification for ZigBee Wireless Sensor Networks in Smart Homes. *IEEE Trans. Instrum. Meas.* **2019**, *68*, 566–575. [[CrossRef](#)]
142. Kim, S.B.; Lee, K.H.; Raj, M.S.; Lee, B.; Reeder, J.T.; Koo, J.; Hourlier-Fargette, A.; Bandodkar, A.J.; Won, S.M.; Sekine, Y.; et al. Soft, Skin-Interfaced Microfluidic Systems with Wireless, Battery-Free Electronics for Digital, Real-Time Tracking of Sweat Loss and Electrolyte Composition. *Small* **2018**, *14*, 1802876. [[CrossRef](#)]
143. Rose, D.P.; Ratterman, M.E.; Griffin, D.K.; Hou, L.; Kelley-Loughnane, N.; Naik, R.R.; Hagen, J.A.; Papautsky, I.; Heikenfeld, J.C. Adhesive RFID Sensor Patch for Monitoring of Sweat Electrolytes. *IEEE Trans. Biomed. Eng.* **2015**, *62*, 1457–1465. [[CrossRef](#)]
144. Baumbauer, C.L.; Anderson, M.G.; Ting, J.; Sreekumar, A.; Rabaey, J.M.; Arias, A.C.; Thielens, A. Printed, flexible, compact UHF-RFID sensor tags enabled by hybrid electronics. *Sci. Rep.* **2020**, *10*, 16543. [[CrossRef](#)]
145. Bassoli, M.; Bianchi, V.; De Munari, I. A plug and play IoT Wi-Fi smart home system for human monitoring. *Electronics* **2018**, *7*, 200. [[CrossRef](#)]

146. Zhang, X.; Grajal, J.; Vazquez-Roy, J.L.; Radhakrishna, U.; Wang, X.; Chern, W.; Zhou, L.; Lin, Y.; Shen, P.C.; Ji, X.; et al. Two-dimensional MoS₂-enabled flexible rectenna for Wi-Fi-band wireless energy harvesting. *Nature* **2019**, *566*, 368–372. [[CrossRef](#)] [[PubMed](#)]
147. Malik, H.; Alam, M.M.; Le Moullec, Y.; Kuusik, A. NarrowBand-IoT Performance Analysis for Healthcare Applications. *Procedia Comput. Sci.* **2018**, *130*, 1077–1083. [[CrossRef](#)]
148. Reeder, J.T.; Choi, J.; Xue, Y.; Gutruf, P.; Hanson, J.; Liu, M.; Ray, T.; Bandodkar, A.J.; Avila, R.; Xia, W.; et al. Waterproof, electronics-enabled, epidermal microfluidic devices for sweat collection, biomarker analysis, and thermography in aquatic settings. *Sci. Adv.* **2019**, *5*, eaau6356. [[CrossRef](#)] [[PubMed](#)]
149. Koh, A.; Kang, D.; Xue, Y.; Lee, S.; Pielak, R.M.; Kim, J.; Hwang, T.; Min, S.; Banks, A.; Bastien, P.; et al. A soft, wearable microfluidic device for the capture, storage, and colorimetric sensing of sweat. *Sci. Transl. Med.* **2016**, *8*, 366ra165. [[CrossRef](#)]
150. Heikenfeld, J.; Jajack, A.; Rogers, J.; Gutruf, P.; Tian, L.; Pan, T.; Li, R.; Khine, M.; Kim, J.; Wang, J.; et al. Wearable sensors: Modalities, challenges, and prospects. *Lab Chip* **2018**, *18*, 217–248. [[CrossRef](#)]
151. Brueck, A.; Iftekhar, T.; Stannard, A.B.; Yelamarthi, K.; Kaya, T. A Real-Time Wireless Sweat Rate Measurement System for Physical Activity Monitoring. *Sensors* **2018**, *18*, 533. [[CrossRef](#)]
152. Barua, A.; Al Alamin, M.A.; Hossain, M.S.; Hossain, E. Security and Privacy Threats for Bluetooth Low Energy in IoT and Wearable Devices: A Comprehensive Survey. *IEEE Open J. Commun. Soc.* **2022**, *3*, 251–281. [[CrossRef](#)]
153. Wen, C.; Dematties, D.; Zhang, S.L. A Guide to Signal Processing Algorithms for Nanopore Sensors. *ACS Sens.* **2021**, *6*, 3536–3555. [[CrossRef](#)]
154. Saeedi, P.; Petersohn, I.; Salpea, P.; Malanda, B.; Karuranga, S.; Unwin, N.; Colagiuri, S.; Guariguata, L.; Motala, A.A.; Ogurtsova, K.; et al. Global and regional diabetes prevalence estimates for 2019 and projections for 2030 and 2045: Results from the International Diabetes Federation Diabetes Atlas, 9th edition. *Diabetes Res. Clin. Pract.* **2019**, *157*, 107843. [[CrossRef](#)]
155. Bailey, T.; Bode, B.W.; Christiansen, M.P.; Klaff, L.J.; Alva, S. The Performance and Usability of a Factory-Calibrated Flash Glucose Monitoring System. *Diabetes Technol. Ther.* **2015**, *17*, 787–794. [[CrossRef](#)]
156. Bertachi, A.; Viñals, C.; Biagi, L.; Contreras, I.; Vehí, J.; Conget, I.; Giménez, M. Prediction of nocturnal hypoglycemia in adults with type 1 diabetes under multiple daily injections using continuous glucose monitoring and physical activity monitor. *Sensors* **2020**, *20*, 1705. [[CrossRef](#)]
157. Yadav, J.; Rani, A.; Singh, V.; Murari, B.M. Investigations on multisensor-based noninvasive blood glucose measurement system. *J. Med. Devices Trans. ASME* **2017**, *11*, 031006. [[CrossRef](#)]
158. Staples, E.; Ingram, R.J.M.; Atherton, J.C.; Robinson, K. Optimising the quantification of cytokines present at low concentrations in small human mucosal tissue samples using Luminex assays. *J. Immunol. Methods* **2013**, *394*, 1–9. [[CrossRef](#)] [[PubMed](#)]
159. Choi, D.H.; Kitchen, G.; Kim, J.S.; Li, Y.; Kim, K.; Jeong, I.C.; Nguyen, J.; Stewart, K.J.; Zeger, S.L.; Searson, P.C. Two Distinct Types of Sweat Profile in Healthy Subjects While Exercising at Constant Power Output Measured by a Wearable Sweat Sensor. *Sci. Rep.* **2019**, *9*, 17877. [[CrossRef](#)]
160. Sabilla, I.A.; Cahyaningtyas, Z.A.; Sarno, R.; Al Fauzi, A.; Wijaya, D.R.; Gunawan, R. Classification of Human Gender from Sweat Odor using Electronic Nose with Machine Learning Methods. In Proceedings of the 2021 IEEE Asia Pacific Conference on Wireless and Mobile (APWiMob), Bandung, Indonesia, 8–9 April 2021; pp. 109–115. [[CrossRef](#)]
161. Sabilla, I.A.; Purbawa, D.P.; Sarno, R.; Al Fauzi, A.; Wijaya, D.R.; Gunawan, R. Men and Women Classification at Night through the Armpit Sweat Odor using Electronic Nose. In Proceedings of the 2021 IEEE Asia Pacific Conference on Wireless and Mobile (APWiMob), Bandung, Indonesia, 8–9 April 2021; pp. 121–127. [[CrossRef](#)]
162. Sabilla, I.A.; Irawan, R.A.; Sarno, R.; Al Fauzi, A.; Wijaya, D.R.; Gunawan, R. Classification of Male and Female Sweat Odor in the Morning Using Electronic Nose. In Proceedings of the 2021 3rd East Indonesia Conference on Computer and Information Technology (EIConCIT), Surabaya, Indonesia, 9–11 April 2021; pp. 320–324.
163. Sankhala, D.; Sardesai, A.U.; Pali, M.; Lin, K.C.; Jagannath, B.; Muthukumar, S.; Prasad, S. A machine learning-based on-demand sweat glucose reporting platform. *Sci. Rep.* **2022**, *12*, 2442. [[CrossRef](#)] [[PubMed](#)]
164. Shahub, S.; Upasham, S.; Ganguly, A.; Prasad, S. Machine learning guided electrochemical sensor for passive sweat cortisol detection. *Sens. Bio-Sens. Res.* **2022**, *38*, 100527. [[CrossRef](#)]
165. Veeralingam, S.; Khandelwal, S.; Badhulika, S. AI/ML-Enabled 2-D—Ru₂ Nanomaterial-Based Multifunctional, Low Cost, Wearable Sensor Platform for Non-Invasive Point of Care Diagnostics. *IEEE Sens. J.* **2020**, *20*, 8437–8444. [[CrossRef](#)]
166. Kalasin, S.; Sangnuang, P.; Surareungchai, W. Satellite-Based Sensor for Environmental Heat-Stress Sweat Creatinine Monitoring: The Remote Artificial Intelligence-Assisted Epidermal Wearable Sensing for Health Evaluation. *ACS Biomater. Sci. Eng.* **2021**, *7*, 322–334. [[CrossRef](#)]
167. Kalasin, S.; Sangnuang, P.; Surareungchai, W. Intelligent Wearable Sensors Interconnected with Advanced Wound Dressing Bandages for Contactless Chronic Skin Monitoring: Artificial Intelligence for Predicting Tissue Regeneration. *Anal. Chem.* **2022**, *94*, 6842–6852. [[CrossRef](#)]
168. Kammarchedu, V.; Butler, D.; Ebrahimi, A. A machine learning-based multimodal electrochemical analytical device based on eMoS_x-LIG for multiplexed detection of tyrosine and uric acid in sweat and saliva. *Anal. Chim. Acta* **2022**, *1232*, 340447. [[CrossRef](#)]
169. Kalasin, S.; Sangnuang, P.; Surareungchai, W. Lab-on-Eyeglasses to Monitor Kidneys and Strengthen Vulnerable Populations in Pandemics: Machine Learning in Predicting Serum Creatinine Using Tear Creatinine. *Anal. Chem.* **2021**, *93*, 10661–10671. [[CrossRef](#)]

170. Hanitra, I.N.; Criscuolo, F.; Carrara, S.; De Micheli, G. Multi-Ion-Sensing Emulator and Multivariate Calibration Optimization by Machine Learning Models. *IEEE Access* **2021**, *9*, 46821–46836. [[CrossRef](#)]
171. Ravizza, A.; De Maria, C.; Di Pietro, L.; Sternini, F.; Audenino, A.L.; Bignardi, C. Comprehensive Review on Current and Future Regulatory Requirements on Wearable Sensors in Preclinical and Clinical Testing. *Front. Bioeng. Biotechnol.* **2019**, *7*, 313. [[CrossRef](#)] [[PubMed](#)]
172. Sun, T.; Hui, J.; Zhou, L.; Lin, B.; Sun, H.; Bai, Y.; Zhao, J.; Mao, H. A low-cost and simple-fabricated epidermal sweat patch based on “cut-and-paste” manufacture. *Sens. Actuators B Chem.* **2022**, *368*, 132184. [[CrossRef](#)]

Disclaimer/Publisher’s Note: The statements, opinions and data contained in all publications are solely those of the individual author(s) and contributor(s) and not of MDPI and/or the editor(s). MDPI and/or the editor(s) disclaim responsibility for any injury to people or property resulting from any ideas, methods, instructions or products referred to in the content.